Production of neutral strange particles K_S^0 and Λ^0 by 12-GeV protons on nuclear targets

F. Abe,* K. Hara,† S. Kim, K. Kondo, S. Miyashita, I. Nakano,
K. Takikawa, R. Tanaka,‡ Y. Yamamoto, T. Yasuda,§ and K. Yasuoka**
Institute of Physics, University of Tsukuba, Sakura-mura, Ibaraki-ken 305, Japan

Y. Fukui
National Laboratory for High Energy Physics (KEK), Oho-machi, Ibaraki-ken 305, Japan
(Received 10 March 1987)

Cross sections for the inclusive processes $p + A \to K_S^0 + X$ and $p + A \to \Lambda^0 + X$ (A=Be, Cu, and W) have been measured for incident protons at 12 GeV. Data are obtained at five laboratory production angles of 3.5°, 5.0°, 6.5°, 8.0°, and 9.5°, covering the kinematic range $0.3 \le x_F \le 0.8$ and $0.4 \le p_T \le 1.3$ GeV/c for K_S^0's and $0.2 \le x_F \le 0.9$ and $0.4 \le p_T \le 1.7$ GeV/c for Λ^0's. The results are discussed in terms of the p_T dependence, the x_F dependence, the A dependence, the cross-section ratio K_S^0/Λ^0, and triple-Regge behavior. The A dependence of K_S^0 and Λ^0 spectra is analyzed in the constituent-quark model. The average ${p_T}^2$'s of quarks and diquarks involved in the K_S^0 and Λ^0 production processes are discussed.

I. INTRODUCTION

Particle production in hadron-nucleus collisions at high energies has been studied extensively.[1] The motivations for studying the A dependence (the effects of the atomic mass A of a heavy nucleus on the production of particles) are largely based on the intuitive expectation that collisions on nuclei may reveal certain aspects of hadronic processes which cannot readily be deduced from collisions on nucleons. For example, early evolution of the hadronic state newly formed in the collision can be probed by allowing the newly formed state to interact with nuclear matter. Recently, several authors[2–9] have applied the constituent-quark models to hadron-nucleus collisions, with a considerable amount of success in describing particle spectra in the projectile-fragmentation region. When analyzed in the constituent-quark models, the A dependence can be used to obtain information on the fragmentation and recombination mechanisms in hadronization.[4,9]

In this paper we report on an experimental study of inclusive K_S^0 and Λ^0 production by 12-GeV protons on Be, Cu, and W targets. The production of K_S^0's and Λ^0's induced by proton beam involves the s quark newly created in the reaction. Using the s quark as a label allows these two reactions to be analyzed with a relatively simple picture of particle production. Previous data on the A dependence of K_S^0 and Λ^0 production by protons come from the Fermilab experiment[10–12] for the incident energies of 300 and 400 GeV. These data stimulated several theoretical models[3–7,9,13] of hadron-nucleus collisions in terms of quark-parton pictures.

The work presented here is a continuation of earlier work on inclusive Λ^0 production by 12-GeV protons on nuclei at the KEK proton synchrotron. Previous publications include measurements of Λ^0 production cross sections on Be, Cu, and W targets,[14] and also on polyethylene (CH_2) and C targets, from which the Λ^0 production cross sections on hydrogen are obtained.[15] The polarization of inclusively produced Λ^0's was also studied.[16,17]

A total of 6500 $K_S^0 \to \pi^+\pi^-$ events was detected in the present experiment. The K_S^0's were detected simultaneously with much more copious Λ^0's in order to check our experimental method and to facilitate comparison between the K_S^0 and Λ^0 production cross sections. Data were collected at five production angles of 3.5°, 5.0°, 6.5°, 8.0°, and 9.5°. In terms of the transverse momentum p_T and the Feynman scaling variable x_F of the produced particle, the kinematic range covered in this experiment was $0.4 \le p_T \le 1.3$ GeV/c and $0.3 \le x_F \le 0.8$ for K_S^0's, and $0.4 \le p_T \le 1.7$ GeV/c and $0.2 \le x_F \le 0.9$ for Λ^0's.

In Sec. II we briefly describe the experimental apparatus and procedures, with emphasis on modifications made for detecting K_S^0's. The data reduction is described in Sec. III. In the first half of Sec. IV the results are presented in comparison with other experiments and theoretical models in terms of the p_T dependence, the x_F dependence, the A dependence, the cross-section ratio K_S^0/Λ^0, and triple-Regge behavior. The latter half of Sec. IV is devoted to the analysis of the A dependence of K_S^0 and Λ^0 production cross sections in the constituent-quark model. The distribution functions which describe the probabilities for quarks or diquarks to hadronize into K_S^0 or Λ^0 are determined. Using these distribution functions, we discuss the average ${p_T}^2$'s of quarks and diquarks involved in the production of K_S^0's and Λ^0's. The conclusions are summarized in Sec. V.

II. EXPERIMENTAL APPARATUS AND PROCEDURES

The experiment was performed at the Λ^0 beam line of the KEK 12-GeV proton synchrotron. The beam line and the detection system were described previously.[14,16–18] A neutral beam was defined at an angle of 6.5° with respect to the primary proton beam line by a collimator embedded in a sweeping magnet. The production

angles were varied in the range from 3.5° to 9.5° by deflecting incident protons horizontally and restoring them to the target by two bending magnets. The geometrical solid angle of the collimator was 100 μsr (10 mrad$\times$10 mrad). The beam spot at the target was approximately 6 mm in diameter (full width at half maximum). The physical size of the Be, Cu, and W targets used in the data taking was 30 mm wide, 10 mm high, and 40 mm thick. The beam intensity was typically 2×10^{10} protons per pulse; the beam spill was 0.5 s long with a repetition period of 2.6 s.

A. Detectors

The detection system consisted of two spectrometer magnets (D1 and D2), two sets of multiwire proportional chambers (PC1 and PC2), four sets of multiwire drift chambers (DC1 through DC4), two sets of scintillation hodoscope counters (H1 and H2), and scintillation counters (S1 through S5, and KS2). Figure 1 shows a general layout of the detectors.

The Λ^0 hyperons were identified by detecting the proton and π^- from the $\Lambda^0\to p\pi^-$ decay, and the K_S^0's by detecting the π^+ and π^- from the $K_S^0\to\pi^+\pi^-$ decay. The configuration of double magnetic spectrometers was employed in such a way that momenta of π^- and p from the Λ^0 decay were analyzed by D1 and D2, respectively. D1 had a large aperture 100 cm wide $\times$80 cm high and a bending power of 0.495 T m. D2 had a large bending power of 1.266 T m and an aperture 60 cm wide $\times$40 cm high. Momenta of π^+ and π^- from the K_S^0 decay were analyzed by the large-aperture magnet D1.

Each set of the proportional and drift chambers had four signal planes: X (horizontal), Y (vertical), U (inclined at 45° with respect to X), and V (inclined at 135° with respect to X). The proportional chambers were read out with a serial data transfer system.[19] The drift chambers were read out with a LeCroy 2770A digitizer and DC201A discriminator.

Each of the hodoscope counters H1 and H2 consisted of 16 elements segmented horizontally. An appropriate combination of signals from the hodoscope counter elements was formed and incorporated into the event trigger.

The scintillation counter S1 defined the upstream end of the decay region for K_S^0's and Λ^0's. The downstream end was defined by the counter KS2 for the K_S^0 decay and by the proportional chamber PC1 for the Λ^0 decay. KS2 had a rectangular hole (45 mm$\times$45 mm) at its center so as to make the counter insensitive to neutral beam backgrounds coming down along the collimator axis. The resulting decrease in the acceptance for the $K_S^0\to\pi^+\pi^-$ decay was small and acceptable. The counters S2–S5 were placed along the path of the protons from the Λ^0 decays. Signals from KS2 and S2 were used as timing pulses for the event trigger, the "common stop" pulse for the 2770A digitizer, and various gate signals.

B. Triggers

Two separate triggers were used in the data collection: K as the master trigger for the $K_S^0\to\pi^+\pi^-$ decay and $p\pi$ for the $\Lambda^0\to p\pi^-$ decay. They were defined by

$$K=\overline{S1}\cdot KS2\cdot PC1\cdot HCK\ ,$$

$$p\pi=\overline{S1}\cdot S2\cdot S3\cdot S4\cdot S5\cdot PC1\cdot HC\Lambda\ ,$$

where by $PC1$ we demanded that two or more planes of the proportional chamber $PC1$ should have wire hits. HCK and $HC\Lambda$ were logic signals formed from the hodoscope counter elements. $HC\Lambda$ in the $p\pi$ trigger was a loose two-track requirement that either H1 or H2 should satisfy two-hit patterns expected for the $\Lambda^0\to p\pi^-$ decay. HCK in the K trigger, on the contrary, was a tight two-track requirement that two tracks should pass through those elements of H1 and H2 located at the opposite sides with respect to the neutral beam path. This was intended to reduce background protons from the Λ^0 decay, which predominantly passed through the central area of the hodoscope counters.

The $p\pi$ triggers were scaled down by a factor of $1/N$ by a prescaler. The value of N was chosen to be 1–30, depending on the relative frequency of the $p\pi$ trigger and

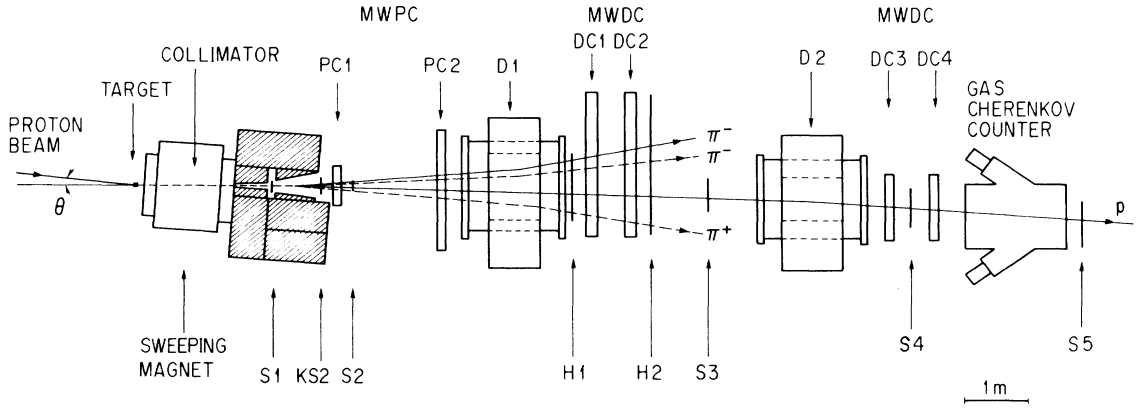

FIG. 1. Plan view of the detection system. Typical trajectories of the daughter proton and pion from the $\Lambda^0\to p\pi^-$ decay are shown by solid lines and those of the daughter pions from the $K_S^0\to\pi^+\pi^-$ decay by dashed lines.

the K trigger. An event was written on tape when the K trigger or the prescaled $p\pi/N$ trigger occurred.

III. DATA REDUCTION

The data reduction was made in the following four steps: (i) Two-track events were selected by a track-finding program and filtered through various cuts to extract $K_S^0 \to \pi^+\pi^-$ and $\Lambda^0 \to p\pi^-$ events; (ii) the detector acceptance was calculated by a Monte Carlo program; (iii) invariant cross sections were calculated from the measured number of events and the estimated acceptance; and (iv) final corrections were applied to the cross sections obtained in (iii).

A. Track finding and cuts

The data were first processed through a track-finding program, the details of which were described in Ref. 17. Tracks were required to lie within given regions of the detectors prescribed for the $K_S^0 \to \pi^+\pi^-$ decay and the $\Lambda^0 \to p\pi^-$ decay. Neutral-vee events in which tracks of opposite charges formed a vertex in the decay region were selected. The vector sum of the two momenta in the neutral-vee events was traced back to the downstream end of the collimator and then to the target, where geometrical cuts were applied.

The main sources of backgrounds in the K trigger were $\gamma \to e^+e^-$ conversions, $\Lambda^0 \to p\pi^-$ decays, and K_L^0 decays into two-charged final states. In order to remove the γ contamination, events were discarded if the opening angle of the two oppositely charged particles was less than 0.02 rad in the laboratory, and also if the invariant mass formed for the hypothesis $\gamma \to e^+e^-$ was less than 50 MeV/c^2. The cut parameters adopted above were determined from distributions of real data and were checked to be consistent with a Monte Carlo simulation.[20] About 14% of the neutral-vee events were rejected by these cuts. The Λ^0 contamination in the K trigger was identified by forming the invariant mass for the hypothesis $\Lambda^0 \to p\pi^-$. Events with the $p\pi^-$ invariant mass less than 1140 MeV/c^2 were removed; they amounted to about 17% of the neutral-vee events. About 60% of the neutral-vee events were removed by the geometrical cut on production points. This cut was efficient for removing the K_L^0 contamination, because about 99.8% of the K_L^0 decay contained missing neutral particles,[21] so that the momentum vector reconstructed from two charged decay products did not point back to the target correctly in most cases. Contaminations from the CP-violating decay $K_L^0 \to \pi^+\pi^-$ were estimated[20] to be negligibly small (less than 1%) by a Monte Carlo simulation.

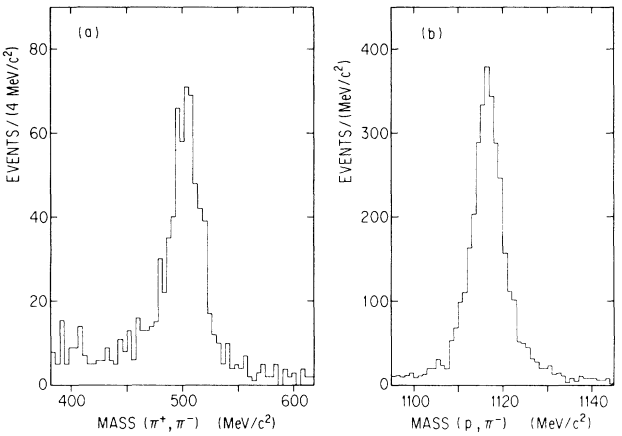

FIG. 2. Typical distributions of (a) the $\pi^+\pi^-$ invariant mass and (b) the $p\pi^-$ invariant mass.

Figure 2(a) shows a typical $\pi^+\pi^-$ invariant-mass distribution for those events which passed the above cuts. The K_S^0 mass peak is formed with a resolution of $\sigma = 12$ MeV/c^2. Events with the $\pi^+\pi^-$ invariant mass within $\pm 3\sigma$ deviations from the mass peak were regarded as K_S^0's. The background under the K_S^0 mass peak was about 15%, which was mainly due to the remnants of the K_L^0 and Λ^0 contaminations.

Contents of the $p\pi$ trigger events were essentially the

TABLE I. The measured numbers of $K_S^0 \to \pi^+\pi^-$ and $\Lambda^0 \to p\pi^-$ events for each target and production angle θ. The ratio of the number of reconstructed events to that of triggers is shown in parentheses.

Target	$\theta = 3.5°$	$\theta = 5.0°$	$\theta = 6.5°$	$\theta = 8.0°$	$\theta = 9.5°$
			$pA \to K_S^0 X$		
Be	411	559	597	385	220
	(0.08%)	(0.14%)	(0.13%)	(0.11%)	(0.10%)
Cu	298	447	584	459	82
	(0.13%)	(0.22%)	(0.25%)	(0.21%)	(0.16%)
W	317	678	604	608	224
	(0.15%)	(0.27%)	(0.32%)	(0.28%)	(0.20%)
			$pA \to \Lambda^0 X$		
Be	11 759	54 197	4775	40 391	4738
	(9.5%)	(12.8%)	(11.7%)	(9.1%)	(5.6%)
Cu	7990	40 306	4273	40 545	6287
	(12.0%)	(16.3%)	(15.4%)	(14.7%)	(9.8%)
W	8388	63 746	3447	37 692	5032
	(12.7%)	(18.1%)	(21.0%)	(17.6%)	(12.9%)

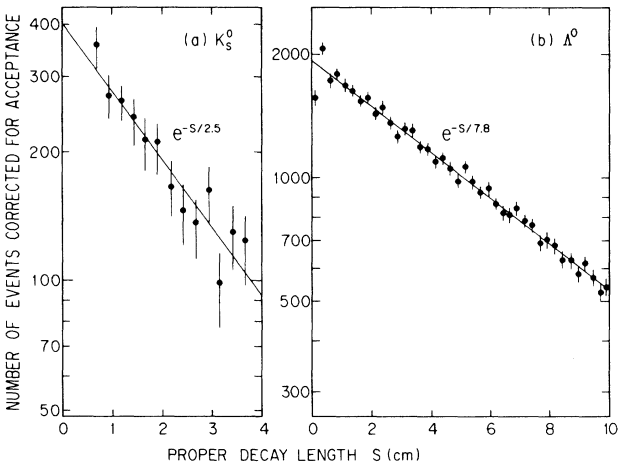

FIG. 3. Distributions of the proper decay length S for (a) the K_S^0 sample at $7.25 \leq p_Z \leq 7.75$ GeV/c and (b) the Λ^0 sample at $8.75 \leq p_Z \leq 9.25$ GeV/c.

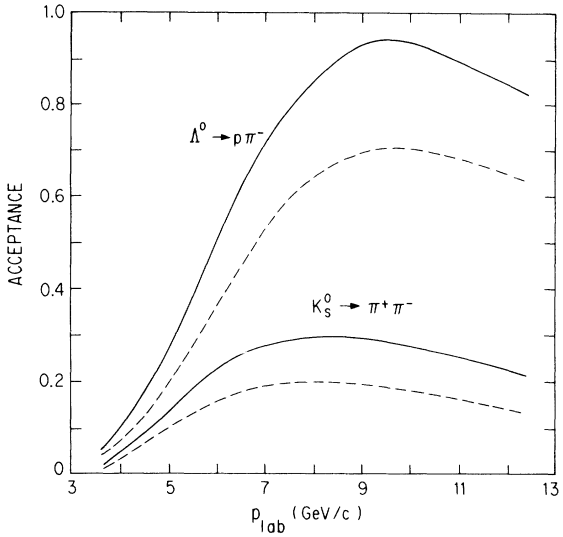

FIG. 4. The detection efficiencies (dashed lines) and the geometrical acceptances (solid lines) for the $K_S^0 \rightarrow \pi^+\pi^-$ decay and the $\Lambda^0 \rightarrow p\pi^-$ decay as a function of the laboratory momentum p_{lab}.

same as in the previous measurement.[17] About 18% of the neutral-vee events were removed by the geometrical cuts at the collimator and the target. The $\gamma \rightarrow e^+e^-$ contamination was about 2% of the neutral-vee events. The $K_S^0 \rightarrow \pi^+\pi^-$ contamination in the $p\pi$ trigger was negligibly small. The $p\pi^-$ invariant mass was formed with a resolution of $\sigma = 3$ MeV/c^2, as shown in Fig. 2(b). The background under the Λ^0 mass peak was about 3%.

The background under the mass peak in the final invariant-mass distribution was subtracted at each momentum bin. The measured numbers of $K_S^0 \rightarrow \pi^+\pi^-$ and $\Lambda^0 \rightarrow p\pi^-$ events are listed in Table I. The background yields detected with the target out were typically 3% in the K_S^0 sample and 2% in the Λ^0 sample. They were subtracted at each bin in the calculation of the cross sections.

As a check of our experimental method, we measured the mean life for the K_S^0 and Λ^0 samples. The proper decay length S of the parent particle was calculated by $S = (Z_{\text{decay}} - Z_{S1})mc/p_Z$, where the Z axis was taken along the collimator axis, Z_{decay} was the Z value of the decay point, Z_{S1} the Z position of the veto counter S1, m the mass of the parent particle, and p_Z the Z component of the laboratory momentum of the parent particle. Typical distributions of S, after being corrected for the acceptance of the detector, are shown in Fig. 3. The mean life determined from the total sample was 2.50 ± 0.15 (7.84 ± 0.05) cm for K_S^0's (Λ^0's) and is in good agreement with the world average[21] of the mean life of K_S^0 (Λ^0), 2.675 (7.89) cm.

B. Monte Carlo calculation of the acceptance

The efficiencies of the present spectrometer system for detecting the $K_S^0 \rightarrow \pi^+\pi^-$ decay and the $\Lambda^0 \rightarrow p\pi^-$ decay were calculated by a Monte Carlo simulation including the following effects: the finite beam size of incident protons, multiple scattering and energy loss of the daughter particles, pion decay in flight, and inefficiencies and spatial resolutions of the tracking chambers.

Monte Carlo events were processed by the track-finding program and filtered through the cut routines in a similar way as real data. The detection efficiency was defined as the ratio of the number of reconstructed events to that of $K_S^0 \rightarrow \pi^+\pi^-$ ($\Lambda^0 \rightarrow p\pi^-$) decays which took place in the decay region. The detection efficiencies as a function of the K_S^0 (Λ^0) laboratory momentum p_{lab} are shown in Fig. 4. Also shown are the geometrical acceptances, which are defined as the fractional number of $K_S^0 \rightarrow \pi^+\pi^-$ ($\Lambda^0 \rightarrow p\pi^-$) decays whose decay products passed through the prescribed area of the detector. The geometrical acceptance for K_S^0's is smaller than that for Λ^0's because of the tight hit-pattern requirement for the hodoscope counters. The geometrical acceptance decreases at lower values of p_{lab} for both K_S^0's and Λ^0's because the acceptance of the spectrometer magnet D1 decreases for pions emitted at large angles with respect to the K_S^0 (Λ^0) direction. The slight decrease at higher p_{lab} is caused by the fact that in the case of the K_S^0 decay high-momentum pions pass through the detectors without hitting the prescribed elements of the hodoscope counters and that in the case of the Λ^0 decay high-momentum protons go down almost straight without hitting the counter S5.

The difference between the geometrical acceptance and the detection efficiency was caused mainly by inefficiencies of the tracking chambers due to the high-intensity primary protons. The uncertainty in the estimation of the detection efficiency was less than 10%.

C. Invariant cross sections

From the measured number of events $N(p_{lab}, \theta)$ at a production angle θ and in a momentum bin Δp at laboratory momentum p_{lab} of K_S^0 (Λ^0), we have calculated the

TABLE II. Target absorption corrections for Λ^0's and K_S^0's: λ_I denotes the nuclear interaction length of protons; λ_T, the nuclear collision length of protons; λ, the mean free path of Λ^0's or K_S^0's; c, the correction factor Eq. (2) for Λ^0's or K_S^0's; $\sigma_{\text{inel}}(K^{\pm}A)$, the inelastic cross sections for $K^{\pm}A$ collisions.

Target	λ_I (Ref. 21) (cm)	λ_T (Ref. 21) (cm)	$\lambda(\Lambda^0)$ (Ref. 14) (cm)	$c(\Lambda^0)$	$\sigma_{\text{inel}}(K^+A)$ (Ref. 22) (mb)	$\sigma_{\text{inel}}(K^-A)$ (Ref. 22) (mb)	$\lambda(K_S^0)$ (cm)	$c(K_S^0)$
Be	36.7	30.0	30±19	1.13±0.05	125±5	146±3	52±10	1.10±0.01
Cu	14.8	9.3	11±2	1.38±0.05	555±30	650±18	16.9±3.4	1.29±0.03
W	10.3	5.6	6.0±0.6	1.69±0.06	1119±91	1410±63	10.9±2.2	1.52±0.07

invariant cross sections for K_S^0 (Λ^0) production by

$$E\frac{d^3\sigma}{dp^3}=\frac{E_{\text{lab}}}{p_{\text{lab}}{}^2}\frac{N(p_{\text{lab}},\theta)}{B\epsilon_{\text{dcy}}A(p_{\text{lab}})\epsilon_{\text{CPU}}\epsilon_{\text{ac}}N_bN_t\Delta\Omega\Delta p}\ , \quad (1)$$

where B is the branching ratio[21] for the $K_S^0\to\pi^+\pi^-$ ($\Lambda^0\to p\pi^-$) decay; ϵ_{dcy} is the probability for the produced K_S^0 (Λ^0) to decay in the decay region; $A(p_{\text{lab}})$ is the detection efficiency defined in Sec. III B; ϵ_{CPU} is the fractional number of event triggers that are written on tape; ϵ_{ac} is the correction for accidental veto rates of the counter S1; N_b is the number of incident protons; N_t is the number of target nuclei per unit area; and $\Delta\Omega$ is the solid angle subtended by the collimator.

During the course of the data collection the number of incident protons N_b was monitored with a secondary-emission chamber and an ionization chamber.[18] The absolute calibration of the proton beam intensity had been made[14] by the activation method of aluminum foil in the previous measurement of Λ^0 production cross sections on Cu at 6.5°. In the present experiment the K_S^0 yield was measured simultaneously with the Λ^0 yield. The absolute scale of the proton beam intensity was determined by normalizing the Λ^0 cross sections to the previously measured values.[14]

D. Corrections

Two final corrections that have to be applied to the cross sections obtained by Eq. (1) are absorption of incident protons and produced particles in the target and a difference between the geometrical and effective solid angles of the collimator.

Assume that the incident protons are absorbed in the target with a mean free path of λ_0 and the produced K_S^0's (Λ^0's) with a mean free path of $\lambda(\Lambda^0)$ ($\lambda(K_S^0)$). The "true" cross section σ is then related to the cross section σ_L that is obtained with a target of length L by $\sigma=c\sigma_L$. Here the absorption correction factor c is given by

$$c=(L/\lambda-L/\lambda_0)/[\exp(-L/\lambda_0)-\exp(-L/\lambda)]\ , \quad (2)$$

where $\lambda=\lambda(\Lambda^0)$ or $\lambda(K_S^0)$.

The Be, Cu, and W targets used in the data collection had a length of $L=40$ mm. The mean free path λ_0 of incident protons was assumed to be given by the nuclear interaction length listed in Ref. 21.

The mean free path $\lambda(\Lambda^0)$ was measured in the previous experiment[14] by comparing Λ^0 yields from two targets of the same material and of different lengths, 40 and 20 mm. The measured values of $\lambda(\Lambda^0)$ were found to be approximately equal to the nuclear collision length of protons rather than the nuclear interaction length (see Table II). Since the nuclear collision length of Λ^0's can be approximated to be equal to that of protons within an accuracy of 10% (Ref. 14), the above result implies that elastic scattering on target nuclei results in the loss of the produced Λ^0's most of the time by deflecting them away from the collimator aperture.

Measurements of the mean free path $\lambda(K_S^0)$ were not made in the present run because of time limitations. Instead, we assumed that $\lambda(K_S^0)$ was given by the nuclear

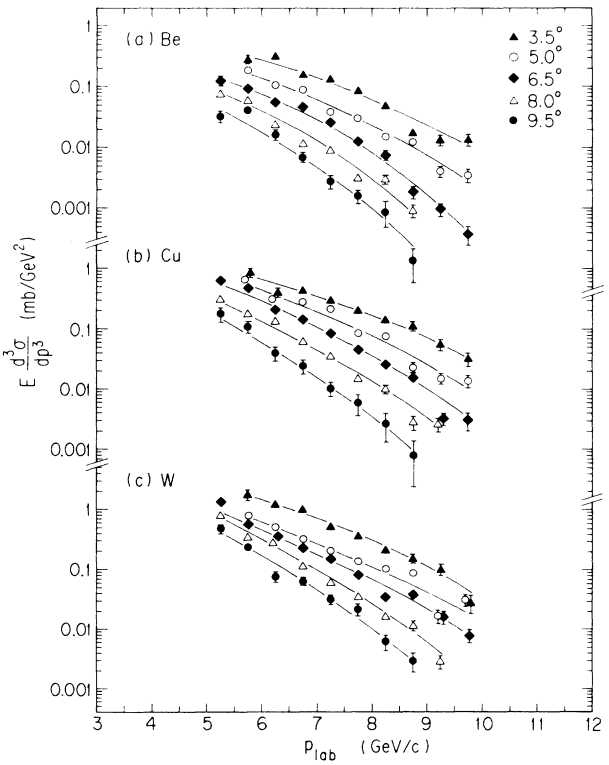

FIG. 5. Invariant cross sections for K_S^0 production by 12-GeV protons on (a) Be, (b) Cu, and (c) W as a function of the laboratory momentum p_{lab} at fixed production angles. The momentum bin width is $\Delta p_{\text{lab}}=0.5$ GeV/c.

collision length of K_S^0's and evaluated the relevant total cross section $\sigma_{\text{tot}}(K_S^0 A)$ for K_S^0-nucleus collisions from existing data[21,22] on $K^{\pm}$-nucleus and $K^{\pm}$-proton collisions. The inelastic cross sections $\sigma_{\text{inel}}(K^{\pm} A)$ for $K^{\pm}$-nucleus collisions are measured by Denisov *et al.*[22] in the energy region of 10 GeV. The ratios of inelastic to total cross sections are known for $K^{\pm}$-proton collisions.[21] Assuming that $\sigma_{\text{tot}}(K_S^0 A)$ is given by a simple average of $K^+ A$ and $K^- A$ total cross sections and that the ratio $\sigma_{\text{inel}}/\sigma_{\text{tot}}$ does not depend on the atomic mass of target nuclei, we calculated $\sigma_{\text{tot}}(K_S^0 A)$ by the expression

$$\sigma_{\text{tot}}(K_S^0 A)=\frac{1}{2}\left[\frac{\sigma_{\text{inel}}(K^+ A)}{0.88}+\frac{\sigma_{\text{inel}}(K^- A)}{0.86}\right], \quad (3)$$

where we put $\sigma_{\text{inel}}(K^+ p)/\sigma_{\text{tot}}(K^+ p)=0.88$ and $\sigma_{\text{inel}}(K^- p)/\sigma_{\text{tot}}(K^- p)=0.86$ in the 5–10-GeV/c momentum range.[21] The results of the absorption correction are summarized in Table II.

The geometrical solid angle of the collimator was 100 μsr, as mentioned in Sec. II. The effective solid angle for K_S^0's was determined by evaluating effects of the finite spread of production points and of scattering and absorption of K_S^0's in the collimator. The collision length of K_S^0's in the collimator, which was made of brass (Zn 40% and Cu 60%), was calculated by Eq. (3). The (x_F, p_T) distribution in K_S^0-nucleus scattering was approximated by the data of Bosetti *et al.*[23] on the $\pi^+ + p \to \pi^+ + X$ reaction at 8 GeV/c. In addition, effects due to K^0 regeneration[24] were also included in the calculation.[20] The regeneration process $K_L^0 \to K_S^0$ increased the effective solid angle by 1.5 μsr at $p_{\text{lab}}=5$ GeV/c, but its effects became negligibly small at higher momenta. These corrections resulted in an effective solid angle of 116 μsr for K_S^0's, essentially independent of p_{lab} in the momentum range of interest. It was 108 μsr for Λ^0's (Ref. 14).

E. Estimation of systematic errors

The major systematic error in the present measurement was an overall uncertainty in the absolute normalization of the cross sections. It consisted of the uncertainty in the proton beam intensity (15%) (Ref. 14), that in the detection efficiency (10%), and that in the collimator solid angle (5%). Adding these uncertainties in quadrature gives an overall uncertainty of 20%.

Fluctuations of the beam conditions gave rise to an angle-to-angle uncertainty of 7%, which was taken into account in the subsequent analyses of the p_T and x_F dependences of the cross sections. The uncertainty in the

TABLE III. Invariant cross sections for K_S^0 production by 12-GeV protons on Be, Cu, and W at production angles 3.5°, 5.0°, 6.5°, 8.0°, and 9.5°. The errors are statistical only.

Angle (deg)	p_T (GeV/c)	x_F	$E\,d^3\sigma/dp^3$ (mb/GeV^2) Be	Cu	W
3.5	0.35	0.50	0.37 ±0.03	1.18 ±0.13	1.69 ±0.18
	0.45	0.64	0.107 ±0.008	0.293 ±0.026	0.554 ±0.045
	0.55	0.78	0.0255±0.0020	0.0920±0.0096	0.121 ±0.012
5.0	0.55	0.53	0.136 ±0.010	0.436 ±0.036	0.527 ±0.037
	0.65	0.63	0.036 ±0.003	0.152 ±0.012	0.191 ±0.013
	0.75	0.72	0.0133±0.0013	0.0451±0.0049	0.0847±0.0066
	0.85	0.82	0.0028±0.0004	0.0091±0.0014	0.0169±0.0022
6.5	0.55	0.38	0.30 ±0.03	1.10 ±0.13	2.20 ±0.24
	0.65	0.46	0.090 ±0.008	0.482 ±0.039	0.645 ±0.058
	0.75	0.53	0.048 ±0.003	0.152 ±0.012	0.259 ±0.020
	0.85	0.61	0.0182±0.0015	0.0646±0.0053	0.114 ±0.010
	0.95	0.68	0.0057±0.0006	0.0240±0.0023	0.0363±0.0037
	1.05	0.76	0.0010±0.0002	0.0059±0.0010	0.0140±0.0022
	1.15	0.83	0.0002±0.0001	0.0009±0.0002	0.0023±0.0007
8.0	0.75	0.40	0.073 ±0.009	0.312 ±0.033	0.666 ±0.063
	0.85	0.46	0.032 ±0.003	0.132 ±0.012	0.278 ±0.023
	0.95	0.52	0.0133±0.0014	0.0603±0.0057	0.1060±0.0094
	1.05	0.58	0.0058±0.0007	0.0234±0.0025	0.0429±0.0041
	1.15	0.63	0.0027±0.0004	0.0105±0.0014	0.0194±0.0024
	1.25	0.69	0.0003±0.0001	0.0017±0.0004	0.0048±0.0009
9.5	0.85	0.35	0.067 ±0.011	0.143 ±0.038	0.419 ±0.073
	0.95	0.40	0.040 ±0.005	0.096 ±0.023	0.244 ±0.031
	1.05	0.45	0.013 ±0.002	0.046 ±0.011	0.056 ±0.009
	1.15	0.49	0.0055±0.0010	0.0143±0.0037	0.0499±0.0074
	1.25	0.54	0.0018±0.0003	0.0090±0.0024	0.0226±0.0037
	1.35	0.58	0.0010±0.0004	0.0043±0.0016	0.0096±0.0024
	1.45	0.63	0.0002±0.0001	0.0007±0.0005	0.0022±0.0007

target absorption correction (5%) and that due to the beam fluctuations (7%) combined to give a target-to-target uncertainty of 9%, which was taken into account in the analysis of the A dependence. The uncertainty in the detection efficiency (10%) and that in the target absorption correction (5%) were taken into account in the analysis of the cross-section ratio K_S^0/Λ^0.

IV. RESULTS AND DISCUSSION

Data were collected at five production angles: 3.5°, 5.0°, 6.5°, 8.0°, and 9.5°. The momentum spectra for K_S^0 production by 12-GeV protons on Be, Cu, and W at the five production angles are shown in Fig. 5. The error bars are statistical only. The curves are drawn to guide the eye.

The numerical values of the K_S^0 production cross sections are listed as a function of the transverse momentum p_T and the Feynman scaling variable x_F in Table III. The x_F is defined by $x_F = p_L^*/p_{\max}^*$, where p_L^* is the longitudinal momentum of the produced particle in the center-of-mass frame of the incident proton and the target and $p_{\max}^*$ is the maximum value of p_L^* that is allowed kinematically. In the calculation of x_F the target is assumed to be a proton at rest. The variables x_F and p_T are mutually related at a fixed production angle θ. The cross sections in Table III were calculated by dividing the data at each production angle θ into p_T bins at intervals of 0.1 GeV/c, with the corresponding value of x_F being calculated from the p_T and θ.

The momentum spectra for Λ^0 production by 12-GeV

TABLE IV. Invariant cross sections for Λ^0 production by 12-GeV protons on Be, Cu, and W at production angles 3.5°, 5.0°, 6.5°, 8.0°, and 9.5°. The errors are statistical only.

Angle (deg)	p_T (GeV/c)	x_F	$E\,d^3\sigma/dp^3$ (mb/GeV^2) Be	Cu	W
3.5	0.25	0.23	1.5 ±0.3	7.9 ±1.6	11.0 ±2.2
	0.35	0.39	1.25 ±0.05	4.80 ±0.23	7.39 ±0.33
	0.45	0.54	0.932 ±0.018	3.173 ±0.072	4.81 ±0.11
	0.55	0.68	0.560 ±0.008	1.662 ±0.031	2.433 ±0.045
	0.65	0.82	0.219 ±0.004	0.625 ±0.014	0.937 ±0.020
5.0	0.45	0.30	1.08 ±0.03	3.87 ±0.11	5.98 ±0.13
	0.55	0.41	0.782 ±0.010	2.688 ±0.037	4.074 ±0.045
	0.65	0.52	0.496 ±0.004	1.631 ±0.016	2.429 ±0.019
	0.75	0.62	0.274 0 ±0.002 2	0.833 6 ±0.007 6	1.281 ±0.009
	0.85	0.72	0.117 5 ±0.001 1	0.353 5 ±0.003 8	0.5548±0.0047
	0.95	0.82	0.035 9 ±0.000 5	0.108 2 ±0.001 7	0.1729±0.0022
	1.05	0.91	0.005 9 ±0.000 2	0.019 5 ±0.000 6	0.0331±0.0008
6.5	0.65	0.34	0.58 ±0.03	2.22 ±0.12	3.84 ±0.22
	0.75	0.42	0.391 ±0.013	1.330 ±0.048	2.227 ±0.092
	0.85	0.50	0.231 ±0.007	0.799 ±0.025	1.411 ±0.048
	0.95	0.57	0.116 ±0.003	0.402 ±0.013	0.636 ±0.024
	1.05	0.65	0.048 8 ±0.001 8	0.186 7 ±0.006 9	0.3112±0.0129
	1.15	0.72	0.018 3 ±0.000 9	0.065 6 ±0.003 4	0.1087±0.0065
	1.25	0.80	0.005 4 ±0.000 4	0.018 5 ±0.001 6	0.0335±0.0031
8.0	0.65	0.21	0.611 ±0.021	2.380 ±0.081	4.428 ±0.155
	0.75	0.28	0.375 ±0.007	1.539 ±0.030	2.598 ±0.054
	0.85	0.34	0.257 ±0.003	1.003 ±0.013	1.758 ±0.025
	0.95	0.41	0.158 6 ±0.001 8	0.600 0 ±0.006 7	1.081 ±0.013
	1.05	0.47	0.089 5 ±0.000 9	0.322 4 ±0.003 5	0.5724±0.0067
	1.15	0.53	0.041 8 ±0.000 5	0.161 1 ±0.001 9	0.2970±0.0037
	1.25	0.59	0.018 9 ±0.000 3	0.072 4 ±0.001 0	0.1321±0.0020
	1.35	0.65	0.007 1 ±0.000 1	0.028 1 ±0.000 5	0.0517±0.0011
	1.45	0.70	0.002 2 ±0.000 1	0.009 1 ±0.000 3	0.0169±0.0005
9.5	0.75	0.17	0.33 ±0.03	1.60 ±0.13	3.04 ±0.29
	0.85	0.23	0.260 ±0.015	1.213 ±0.062	2.154 ±0.123
	0.95	0.28	0.162 ±0.007	0.717 ±0.026	1.315 ±0.054
	1.05	0.33	0.103 ±0.003	0.412 ±0.013	0.791 ±0.027
	1.15	0.38	0.057 7 ±0.001 9	0.237 9 ±0.007 0	0.4542±0.0147
	1.25	0.43	0.028 6 ±0.001 0	0.117 3 ±0.003 7	0.2420±0.0081
	1.35	0.48	0.014 2 ±0.000 6	0.053 8 ±0.002 0	0.1209±0.0045
	1.45	0.53	0.005 8 ±0.000 3	0.026 5 ±0.001 1	0.0486±0.0024
	1.55	0.76	0.000 50±0.000 03	0.002 4 ±0.000 1	0.0050±0.0003
	1.65	0.82	0.000 09±0.000 01	0.000 43±0.000 04	0.0011±0.0001

protons on Be, Cu, and W at 3.5°, 6.5°, and 9.5° were already described in Ref. 14. At these angles, the Λ^0 production cross sections obtained in the present experiment agreed with the previous values[14] within statistical accuracies. In Table IV we list the Λ^0 production cross sections obtained in the present experiment, on which the subsequent analyses presented in this paper are based.

A. p_T dependence

In Fig. 6 we show several of the invariant cross sections for K_S^0 production as a function of p_T at fixed values of x_F. The p_T dependence of the cross sections was fitted to the Gaussian form:

$$E\frac{d^3\sigma}{dp^3}(x_F,p_T)=E\frac{d^3\sigma}{dp^3}(x_F,p_T=0)\exp[-b(x_F)p_T{}^2] \ . \quad (4)$$

The fitted curves are also shown in Fig. 6. This demonstrates that the Gaussian form reproduces the p_T dependence of the data well. The p_T dependence of the Λ^0 production cross sections was also reproduced by the Gaussian form. The angle-to-angle systematic error of 7% was included in the fits. The slope parameters $b(x_F)$ for K_S^0 production are listed in Table V and those for Λ^0 production in Table VI. The cross sections extrapolated to $p_T=0$ by Eq. (4), $E\,d^3\sigma/dp^3(x_F,p_T=0)$, are used in later analyses.

The slope parameters $b(x_F)$ for K_S^0 production are plotted in Fig. 7(a). The data do not appear to depend strongly on x_F in the measured range of x_F. Assuming a flat x_F dependence for each target nucleus yields the aver-

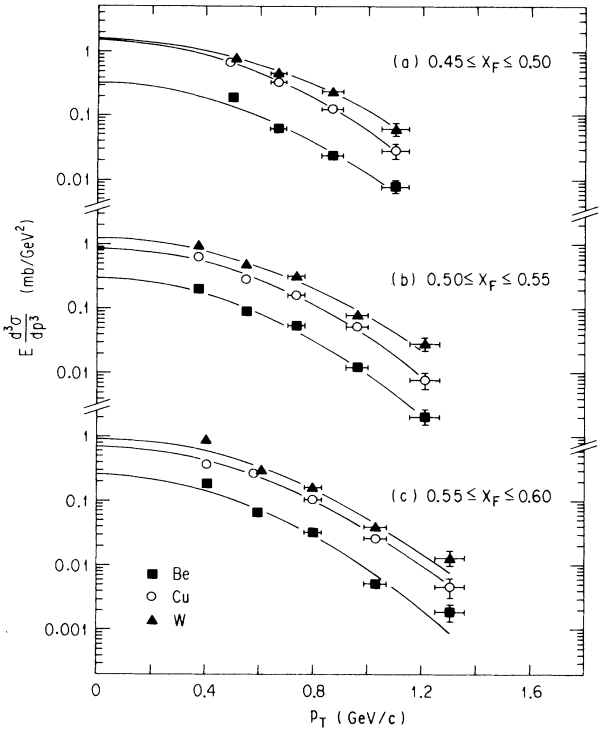

FIG. 6. Invariant cross sections for K_S^0 production by 12-GeV protons on Be, Cu, and W as a function of p_T at fixed x_F: (a) $0.45 \le x_F \le 0.50$, (b) $0.50 \le x_F \le 0.55$, and (c) $0.55 \le x_F \le 0.60$. The curves are the fits given by Eq. (4).

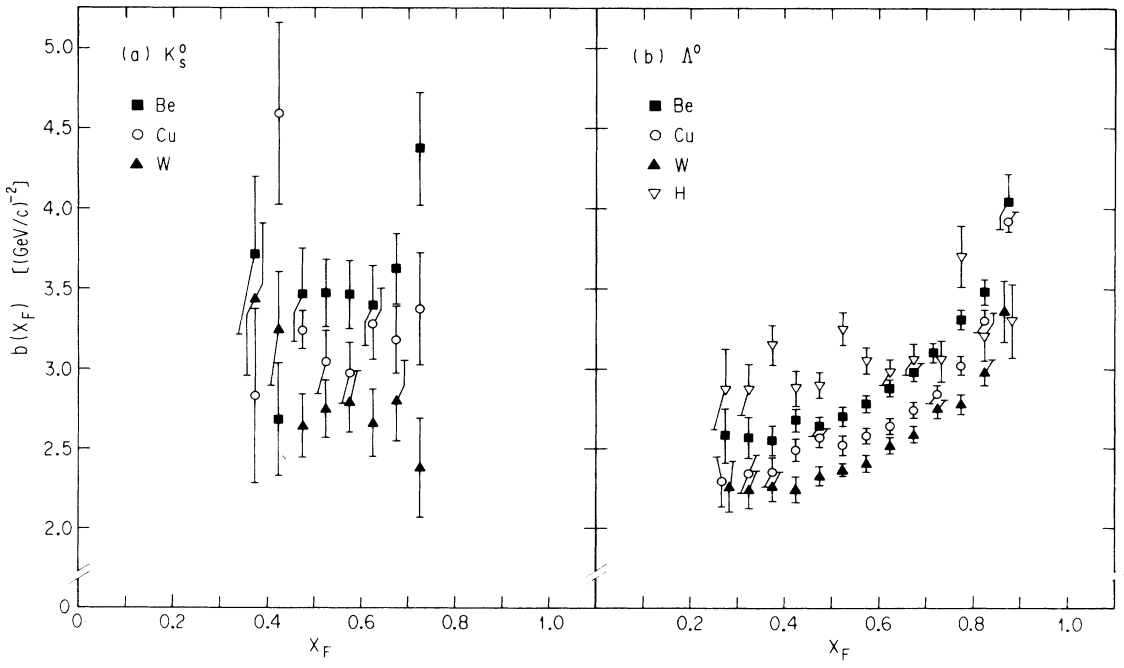

FIG. 7. Slope parameters $b(x_F)$ of the p_T dependence of the invariant cross sections for (a) K_S^0 production and (b) Λ^0 production. The hydrogen data for Λ^0 production (inverted open triangles) are from Ref. 15.

TABLE V. Slope parameters $b(x_F)$ [in $(\text{GeV}/c)^{-2}$] in the p_T dependence of K_S^0 production cross sections by 12-GeV protons on Be, Cu, and W. The errors include the angle-to-angle uncertainty of 7%.

x_F	Be	Cu	W
0.375	3.71±0.49	2.83±0.55	3.43±0.48
0.425	2.68±0.35	4.59±0.57	3.25±0.36
0.475	3.46±0.29	3.24±0.12	2.64±0.20
0.525	3.47±0.21	3.04±0.20	2.75±0.18
0.575	3.46±0.21	2.97±0.19	2.79±0.19
0.625	3.39±0.25	3.28±0.22	2.66±0.21
0.675	3.62±0.22	3.18±0.21	2.80±0.25
0.725	4.37±0.35	3.37±0.35	2.38±0.31

age value of $b(x_F)$ of 3.60±0.08 for Be, 3.29±0.08 for Cu, and 2.83±0.07 $(\text{GeV}/c)^{-2}$ for W. The x_F-averaged slope parameters indicate a trend to decrease with increasing A.

In Fig. 7(b) we plot the slope parameters $b(x_F)$ for Λ^0 production on Be, Cu, and W. Also plotted are the hydrogen data obtained in the previous measurement.[15] The slope parameters $b(x_F)$ for nuclear targets decrease with increasing A over the entire x_F range covered. More importantly, the slope parameters $b(x_F)$ for nuclear targets increase with increasing x_F, while those for hydrogen seem to remain approximately constant in the measured x_F range.

The different x_F behavior of the slope parameters $b(x_F)$ for K_S^0's and Λ^0's deserves attention; this phenomenon will be dealt with in the picture of the constituent-quark model in Sec. IV G.

B. x_F dependence

The x_F dependence of the K_S^0 and Λ^0 production cross sections were fitted to the form

$$E\frac{d^3\sigma}{dp^3} = A(p_T)(x_0 - x_F)^{m(p_T)}, \quad (5)$$

TABLE VI. Slope parameters $b(x_F)$ [in $(\text{GeV}/c)^{-2}$] in the p_T dependence of Λ^0 production cross sections by 12-GeV protons on Be, Cu, and W. The errors include the angle-to-angle uncertainty of 7%.

x_F	Be	Cu	W
0.275	2.58±0.17	2.29±0.16	2.26±0.16
0.325	2.57±0.13	2.34±0.12	2.24±0.12
0.375	2.55±0.09	2.35±0.09	2.26±0.09
0.425	2.68±0.07	2.49±0.07	2.24±0.08
0.475	2.64±0.06	2.57±0.06	2.33±0.06
0.525	2.70±0.06	2.52±0.06	2.37±0.03
0.575	2.78±0.05	2.58±0.05	2.41±0.05
0.625	2.88±0.05	2.64±0.05	2.52±0.05
0.675	2.98±0.06	2.74±0.05	2.59±0.05
0.725	3.10±0.06	2.84±0.06	2.75±0.06
0.775	3.31±0.06	3.02±0.06	2.78±0.06
0.825	3.48±0.08	3.30±0.07	2.98±0.08
0.875	4.04±0.17	3.92±0.06	3.36±0.19

where x_0 is the maximum value of x_F that is allowed kinematically at a given p_T; for example, x_0 at $p_T = 1$ GeV/c is 0.88 (0.89) for K_S^0 (Λ^0) production. The fits were made for several p_T values to investigate possible p_T dependence of the powers m. Equation (5) fits the data well, as demonstrated in Figs. 8(a) and 8(b).

The powers m for K_S^0 production are plotted versus p_T in Fig. 9(a) and those for Λ^0 production in Fig. 9(b). The values at $p_T = 0$ were determined by fitting the extrapolated cross sections $E\,d^3\sigma/dp^3(x_F, p_T = 0)$ to Eq. (5). The powers m for K_S^0 production appear to decrease with increasing p_T, while the p_T dependence of the powers m for Λ^0 production is weak. As for the differences between target nuclei, Fig. 9(b) shows that the powers m for low-p_T Λ^0 production on a heavy nucleus are larger than those on a light nucleus. This is consistent with the nuclear attenuation effect[10,11,14] in forward Λ^0 production; the forward Λ^0 spectrum on a heavy nucleus is attenuated relative to a light nucleus. In the K_S^0 data of Fig. 9(a) this trend is barely seen at $p_T = 0$.

For comparison, other previous data on the powers m are also shown in Figs. 9(a) and 9(b): the data of Ref. 15 for Λ^0 production by 12-GeV protons on hydrogen, the data of Edwards *et al.*[25] for K_S^0 and Λ^0 production by 200-GeV/c protons on Be, and the data of Bobbink *et al.*[26] for Λ^0 production in proton-proton collisions at the CERN ISR. Our results are consistent with these data.

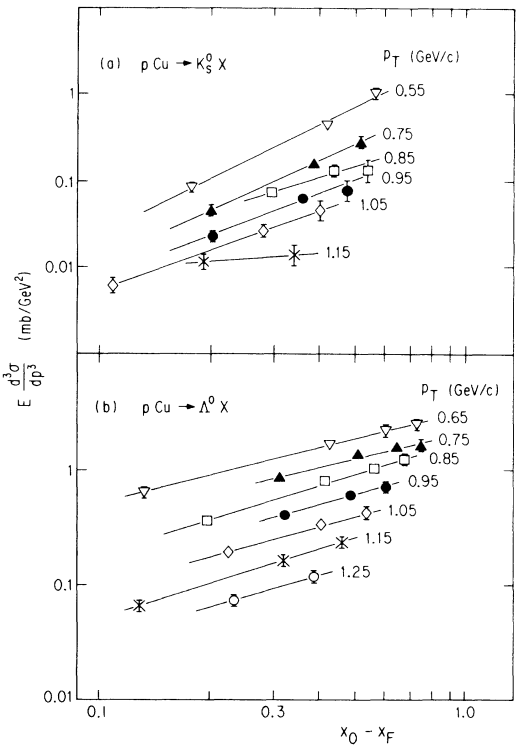

FIG. 8. Plots of the invariant cross sections versus $x_0 - x_F$: (a) $p\text{Cu} \to K_S^0 X$ and (b) $p\text{Cu} \to \Lambda^0 X$. The straight lines are the fits given by Eq. (5).

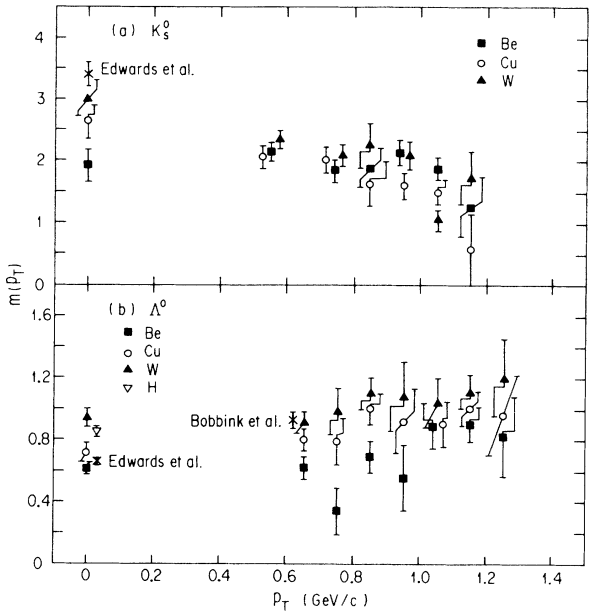

FIG. 9. Powers $m(p_T)$ of the x_F dependence of the invariant cross sections for (a) K_S^0 production and (b) Λ^0 production. The inverted open triangle is the data of Ref. 15 for Λ^0 production by 12-GeV protons on hydrogen. The crosses are the data of Edwards *et al.* (Ref. 25) for K_S^0 and Λ^0 production by 200-GeV/c protons on Be and the data of Bobbink *et al.* (Ref. 26) for Λ^0 production in pp collisions at the CERN ISR.

The power m in the $(1-x_F)^m$ dependence of the forward particle spectrum is related to quark-parton pictures by the quark-counting rules, of which some different versions have been proposed.[27] The latest rule by Gunion[28] is based on gluon exchange rather than quark exchange as the hadronic interaction mechanism and pointlike pair creation as the mechanism for producing sea quarks. The suppression of d quarks as compared to u quarks in proton structure functions in the $x_F \to 1$ limit is taken into account by increasing m by 1 unit. According to this rule, the power m is 4 for the $p \to K_S^0$ fragmentation and 1 for the $p \to \Lambda^0$ fragmentation. These predictions are in qualitative agreement with our data at small p_T.

It should be noted that the quark-counting-rule prediction depends on specific quark processes assumed for the $p \to$hadron fragmentation. The prediction $m=1$ for the $p \to \Lambda^0$ fragmentation applies for the fragmentation of two fast quarks into Λ^0. In addition to this process, the fragmentation of a single fast quark into Λ^0, for which the counting rule predicts $m=3$, has an appreciable contribution to Λ^0 production in proton-nucleus collisions at moderate x_F. The constituent-quark model allows separation of these two processes and hence more detailed comparison with the counting rule (see Sec. IV F).

C. A dependence of K_S^0 production

The A dependence of the K_S^0 production cross sections was fitted to the empirical power law

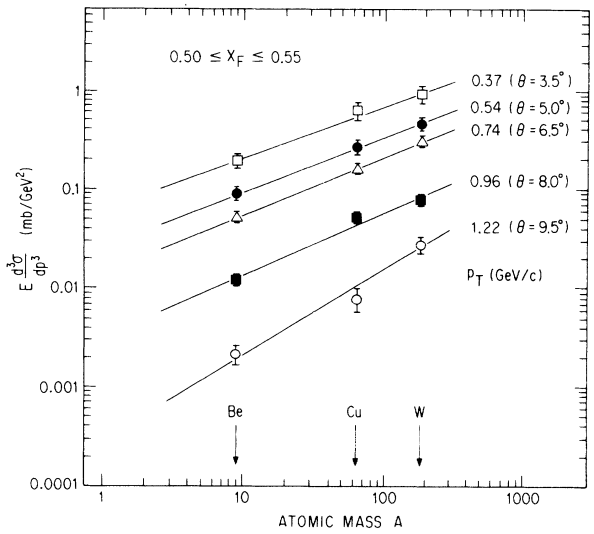

FIG. 10. Typical plots of the K_S^0 production cross sections on Be, Cu, and W as a function of A. The straight lines are the fits given by Eq. (6).

$$E\frac{d^3\sigma}{dp^3}(x_F,p_T;A)=E\frac{d^3\sigma}{dp^3}(x_F,p_T;A=1)A^{\alpha(x_F,p_T)} . \quad (6)$$

In Fig. 10 we plot the cross sections as a function of A for several p_T values at typical x_F, together with the fits given by Eq. (6). The data are well represented by the power-law fit. The cross sections extrapolated to $A=1$ by Eq. (6), $E\,d^3\sigma/dp^3(x_F,p_T;A=1)$, are used later in the triple-Regge analysis (see Sec. IV E).

The exponents $\alpha(x_F,p_T)$ are plotted as a function of p_T at fixed x_F in Fig. 11. Also shown are the data of Skubic *et al.*[11] at 300 GeV. Our data indicate a trend to increase with increasing p_T and are consistent with the data at 300 GeV.

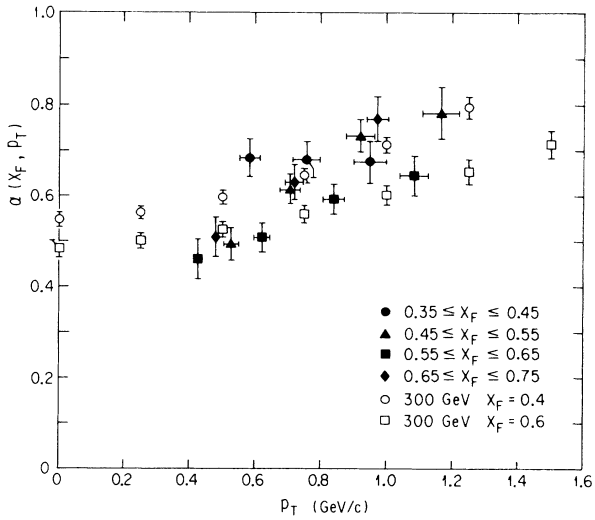

FIG. 11. Exponents $\alpha(x_F,p_T)$ of the A dependence of the K_S^0 production cross sections as a function of p_T at fixed x_F. The data at 300 GeV are from Ref. 11.

The exponents α at $p_T=0$, $\alpha(x_F,p_T=0)$, were calculated by fitting the extrapolated cross sections $E\,d^3\sigma/dp^3(x_F,p_T=0)$ to Eq. (6). The results are plotted in Fig. 12 in comparison with the data[11] at 300 GeV and several model predictions. The nuclear attenuation[10,11,14] in forward hadron production implies that $\alpha(x_F,p_T\simeq 0)<\alpha_0$ for large x_F, where $\alpha_0=0.695$ is the exponent in the power-law fit of proton-nucleus inelastic cross sections.[22] In the framework of the constituent-quark model, Dar and Takagi[5] and Berlad *et al.*[6] predict that $\alpha(x_F,p_T=0)$ for K_S^0 production does not depend on x_F above moderate x_F ($x_F\gtrsim 0.4$). Numerical values predicted by Refs. 5 and 6 are essentially the same for the combination of Be, Cu, and W targets and are shown by the line 1 in Fig. 12. Nikolaev and Pokorski[29] predict weaker attenuation, i.e., larger values of $\alpha(x_F)$ in the additive quark model and stronger attenuation in the collective model. Capella and Tran Thanh Van[30] predict likewise stronger attenuation based on the dual-parton model. Note that all the models mentioned above reproduce the measured behavior of $\alpha(x_F)$ for Λ^0 production[10,11,14] and are not distinguished by the Λ^0 data alone. Our K_S^0 data are consistent with the data[11] at 300 GeV and favor the constituent-quark models of Dar and Takagi and of Berlad *et al.*, the collective model of Nikolaev and Pokorski, and the dual-parton model of Capella and Tran Thanh Van, but do not favor the additive quark model of Nikolaev and Pokorski.

The results for the power-law analysis of the A dependence of the present Λ^0 data were essentially the same as described in Ref. 14.

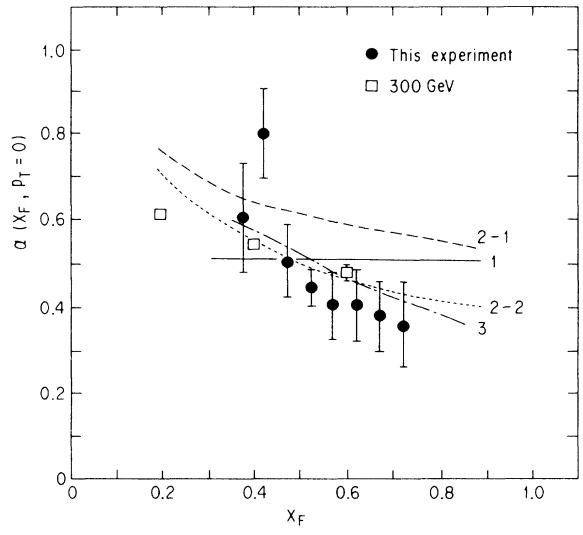

FIG. 12. Exponents $\alpha(x_F,p_T=0)$ of the A dependence of the K_S^0 production cross sections in comparison with the data at 300 GeV (Ref. 11) and theoretical predictions: curve 1, the constituent-quark models of Dar and Takagi (Ref. 5) and Berlad *et al.* (Ref. 6); curve 2-1, the additive quark model of Nikolaev and Pokorski (Ref. 29); curve 2-2, the collective model of the same authors; curve 3, the dual-parton model of Capella and Tran Thanh Van (Ref. 30).

D. Cross-section ratio K_S^0/Λ^0

The ratio of the invariant cross section for K_S^0 production to that for Λ^0 production is plotted against A for typical x_F and p_T values in Fig. 13. For given values of x_F at fixed θ, the corresponding p_T values are different for K_S^0 production and Λ^0 production. The K_S^0/Λ^0 ratios as a function of x_F and p_T were calculated by interpolating or extrapolating the cross sections according to the Gaussian p_T dependence at each x_F. Figure 13 shows that the K_S^0/Λ^0 ratio does not depend strongly on A and that the ratio decreases at higher x_F and p_T.

The K_S^0/Λ^0 ratios in terms of the p_T-integrated cross sections were fitted to a simple exponential function of x_F:

$$\int E\frac{d^3\sigma}{dp^3}(p\to K_S^0)dp_T{}^2 \Big/ \int E\frac{d^3\sigma}{dp^3}(p\to\Lambda^0)dp_T{}^2 = a\exp(-bx_F)\ . \quad (7)$$

The parameters a (b) obtained are $a=1.34\pm0.37$ ($b=7.03\pm0.65$) for Be, $a=1.08\pm0.41$ ($b=5.61\pm0.72$) for Cu, and $a=1.22\pm0.34$ ($b=5.89\pm0.65$) for W, indicating that the K_S^0/Λ^0 ratio does not depend strongly on A.

The p_T-integrated cross-section ratios K_S^0/Λ^0 for Be are plotted versus x_F in Fig. 14 in comparison with other experiments. Skubic *et al.*[11] report that the K_S^0/Λ^0 ratio in proton-nucleus collisions at 300 GeV is described by the function $2.99\exp(-6.45x_F)$ in the range $0.2\le x_F\le 0.7$, irrespective of p_T between 0 and 2 GeV/c, and that the ratio does not depend strongly on target nucleus, Be or Pb. Their results are shown by the dashed line in Fig. 14. Figure 14 shows that the x_F dependence of the K_S^0/Λ^0 ratio obtained in the present experiment is consistent with previous experiments.[11,25,31,32]

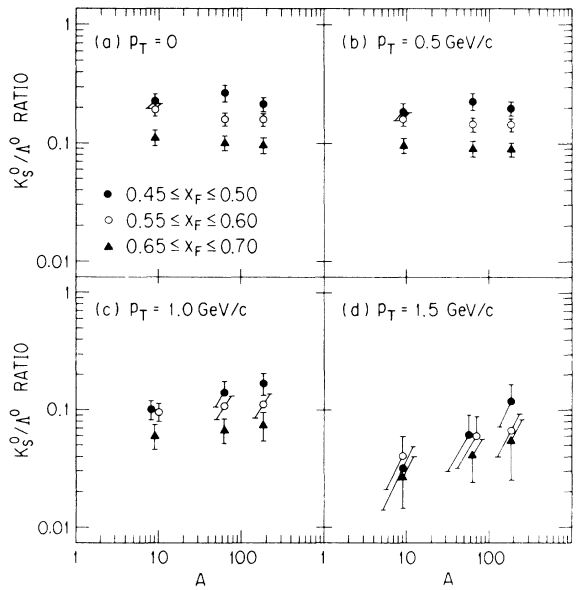

FIG. 13. Cross-section ratios K_S^0/Λ^0 as a function of A for typical x_F bins at (a) $p_T=0$, (b) $p_T=0.5$, (c) $p_T=1.0$, and (d) $p_T=1.5$ GeV/c.

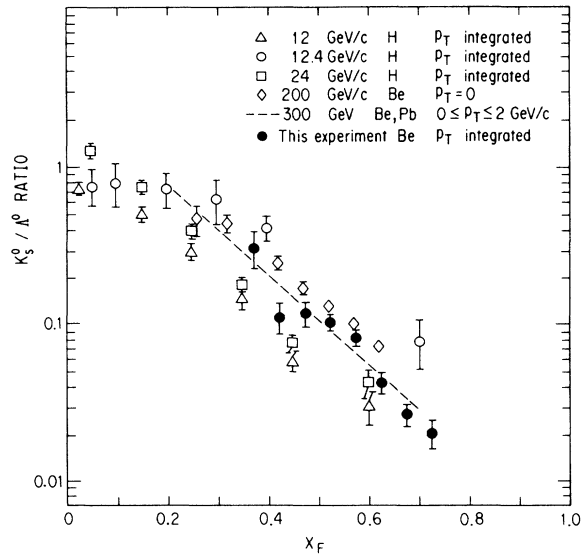

FIG. 14. The p_T-integrated cross section ratios K_S^0/Λ^0 versus x_F in comparison with other experiments. Data are taken from the following references: open triangles and open squares, Ref. 31; open circles, Ref. 32; open diamonds, Ref. 25; dashed line, Ref. 11.

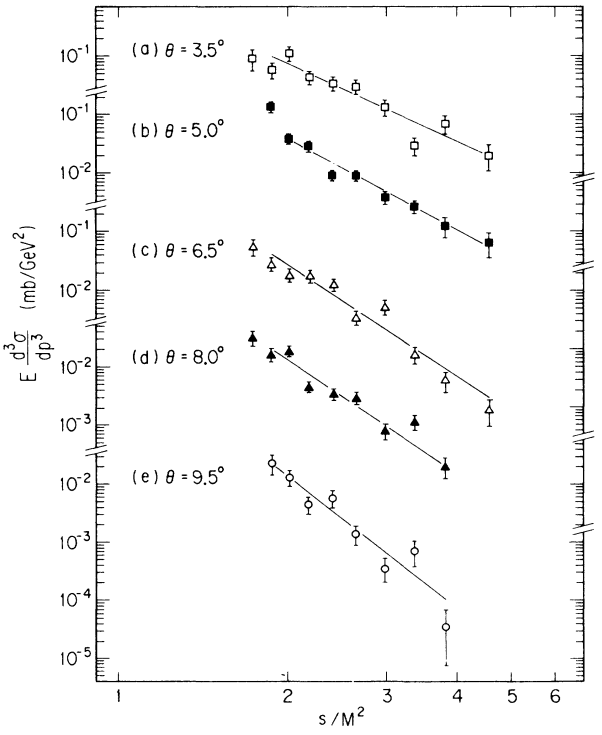

FIG. 15. The $A = 1$ extrapolated cross sections for K_S^0 production as a function of s/M^2 at fixed production angles. The straight lines are the fits to data points.

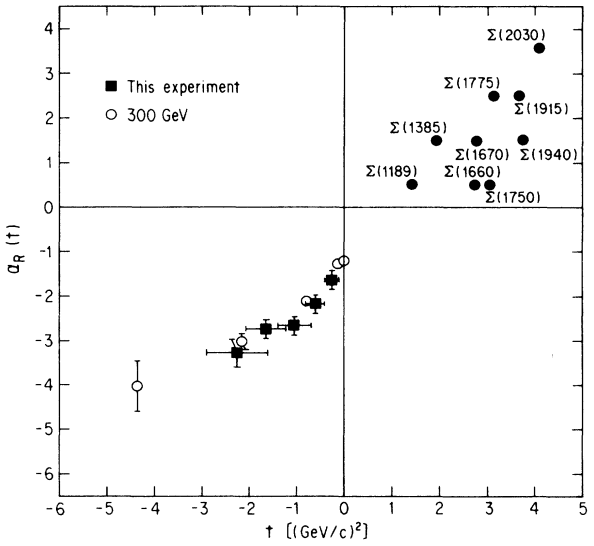

FIG. 16. Effective Regge trajectory $\alpha_R(t)$ for K_S^0 production. The data at 300 GeV are from Ref. 35.

E. Triple-Regge analysis of K_S^0 production

The triple-Regge model[33,34] is one of the successful phenomenological theories of inclusive particle production at low p_T. In this model the invariant cross section for inclusive K_S^0 production at c.m. energy $\sqrt{s}$ is written[34] in terms of the missing mass squared M^2 and the four-momentum transfer squared t by the expression

$$E\frac{d^3\sigma}{dp^3}(M^2,t) = \frac{G(t)}{\pi}\left[\frac{M^2}{s}\right]^{1-2\alpha_R(t)}, \tag{8}$$

where $G(t)$ is the residue function and $\alpha_R(t)$ is the effective Regge trajectory.

The $A = 1$ extrapolated cross sections that were ob-

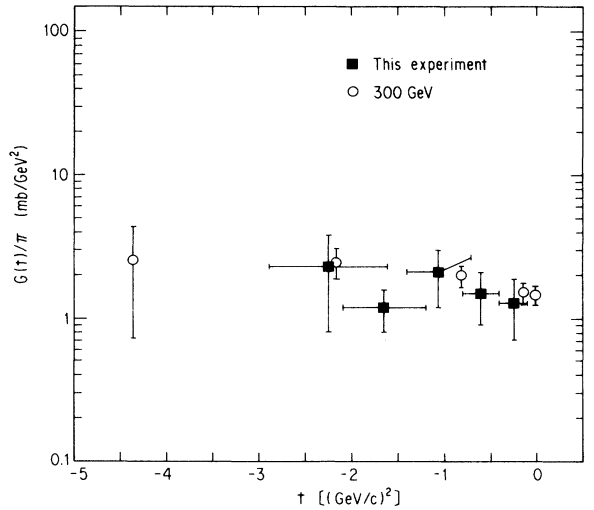

FIG. 17. Residue function $G(t)$ divided by π for K_S^0 production. The data at 300 GeV are from Ref. 35.

TABLE VII. Results of the triple-Regge analysis of the $A=1$ extrapolated cross sections for K_S^0 production. The errors are statistical only. The last column indicates the χ^2 values divided by the number of degrees of freedom.

θ (deg)	t [(GeV/c)^2]	$\alpha_R(t)$	$G(t)/\pi$ (mb/GeV^2)	χ^2/DF
3.5	$-0.4 \le t \le -0.1$	-1.64 ± 0.21	1.3 ± 0.6	14/7
5.0	$-0.8 \le t \le -0.4$	-2.17 ± 0.20	1.5 ± 0.6	3/6
6.5	$-1.4 \le t \le -0.7$	-2.69 ± 0.21	2.1 ± 0.9	15/7
8.0	$-2.1 \le t \le -1.2$	-2.74 ± 0.21	1.2 ± 0.4	21/7
9.5	$-2.9 \le t \le -1.6$	-3.27 ± 0.33	2.3 ± 1.5	12/6

tained in Eq. (6) were fitted to Eq. (8) under the assumption that $G(t)$ and $\alpha_R(t)$ were constants at each production angle θ. In Fig. 15 we plot the $A=1$ extrapolated cross sections as a function of s/M^2 at fixed production angles. The data are well reproduced by the straight-line fit. The results of the fits are summarized in Table VII. The range of t at each θ is indicated as a bin width of t in the table.

The $\alpha_R(t)$ and $G(t)/\pi$ are plotted versus t in Figs. 16 and 17 in comparison with the data of Devlin *et al.*[35] at 300 GeV. Their data refer to the $A=1$ extrapolated cross sections determined from Be and Pb data. Also plotted are some Σ states which may contribute to the reaction $pp \to K_S^0 X$ as the Reggeon. The present results on $\alpha_R(t)$ and $G(t)$ are consistent with the data at 300 GeV. Both of them seem to lie between $\Sigma_\alpha - \Sigma_\gamma$ trajectory [$\Sigma(1189)$, $\Sigma(1670)$, and $\Sigma(1915)$] and $\Sigma'_\alpha - \Sigma'_\gamma$ trajectory [$\Sigma(1750)$ and $\Sigma(1940)$], which are the natural-parity trajectories.[34,36]

The results for the triple-Regge analysis of the present Λ^0 data were essentially the same as described in Ref. 14.

F. Analysis in the constituent-quark model

Recently several authors[2–9] have shown that the constituent-quark models provide a reasonable description of many features of low-p_T hadron-nucleus collisions. The basic picture of the models as applied to the projectile fragmentation in proton-nucleus collisions can be summarized as follows. (1) A nucleon is viewed as a system of 3 spatially separated constituent quarks, each containing a valence quark and a virtual cloud of sea quarks and gluons. (2) When an incident proton collides with a nucleus, one, two, or three constituent quarks in the incident proton are "wounded," i.e., interact inelastically with target quarks and lose a considerable fraction of their initial momenta. The number of wounded quarks in the incident proton would usually be one in a proton-nucleon collision, while in a proton-nucleus collision an increasing number of constituent quarks are wounded with an increasing size of the target nucleus or A. (3) The remaining constituent quarks in the incident proton which were not wounded pass through the nucleus, retaining their initial momenta, and hadronize through fragmentation or recombination to form fast hadrons. They are called leading quarks. The spectra in the projectile-fragmentation region $x_F \gtrsim 0.2$ are dominated by contributions from the leading quarks. The wounded quarks predominantly contribute to the spectra in the central rapidity region.

According to the above picture, the Λ^0 production cross section in the projectile-fragmentation region of proton-nucleus (pA) collisions is written[3,5,6,9] by the expression

$$\frac{1}{\sigma_{pA}} E \frac{d^3\sigma}{dp^3}(x_F, p_T; A) = P_{pA}^{(1)} f^{(1)}_{p\to\Lambda^0}(x_F, p_T) + P_{pA}^{(2)} f^{(2)}_{p\to\Lambda^0}(x_F, p_T) \ , \quad (9)$$

where σ_{pA} is the total inelastic cross section for pA collisions, $P_{pA}^{(i)}$ is the probability that i constituent quarks in the incident proton are wounded in nucleus A, and $f^{(i)}_{p\to\Lambda^0}(x_F, p_T)$ is the (x_F, p_T) distribution of Λ^0's that are produced in the fragmentation or recombination of the remaining $(3-i)$ leading quarks. The probability $P_{pA}^{(i)}$ depends on A, but not on the final-state particle observed. The distribution function $f^{(i)}_{p\to\Lambda^0}(x_F, p_T)$ of the final-state particle is independent of A.

Optical-model calculations with the help of the quark additivity approximation give[9]

$$P_{pA}^{(1)} = 3(\sigma_{pA} - \sigma_{\pi A})/\sigma_{pA} \ , \quad (10a)$$

$$P_{pA}^{(2)} = 3(3\sigma_{\pi A} - \sigma_{pA} - \sigma_{qA})/\sigma_{pA} \ , \quad (10b)$$

$$P_{pA}^{(3)} = 1 - P_{pA}^{(1)} - P_{pA}^{(2)} \ , \quad (10c)$$

where σ_{pA}, $\sigma_{\pi A}$, and σ_{qA} are inelastic pA, πA, and qA cross sections, respectively. If some reasonable estimation of $P_{pA}^{(i)}$ or a set of cross sections σ_{pA}, $\sigma_{\pi A}$, and σ_{qA} is available, one can determine the distributions $f^{(i)}_{p\to\Lambda^0}(x_F, p_T)$ from experimental data on the A dependence. Takagi[9] analyzed the Fermilab data[11,12] on forward Λ^0 and Ξ^0 production by 300-GeV protons on nuclei by using the cross section data σ_{pA} and $\sigma_{\pi A}$ of Denisov *et al.*[22] for the incident energies of 20–60 GeV and by estimating σ_{qA} by means of optical-model formulas applied at the constituent-quark level with the simple uniform-disk approximation for quark densities in nuclei.

TABLE VIII. The A-dependent parameters σ_{pA} and $P_{pA}^{(i)}$ in the constituent-quark model of Takagi (adapted from Ref. 9).

Target	σ_{pA}(mb)	$P_{pA}^{(1)}$	$P_{pA}^{(2)}$
Be	206.8	0.846	0.146
Cu	808.1	0.585	0.347
W	1684.8	0.439	0.425

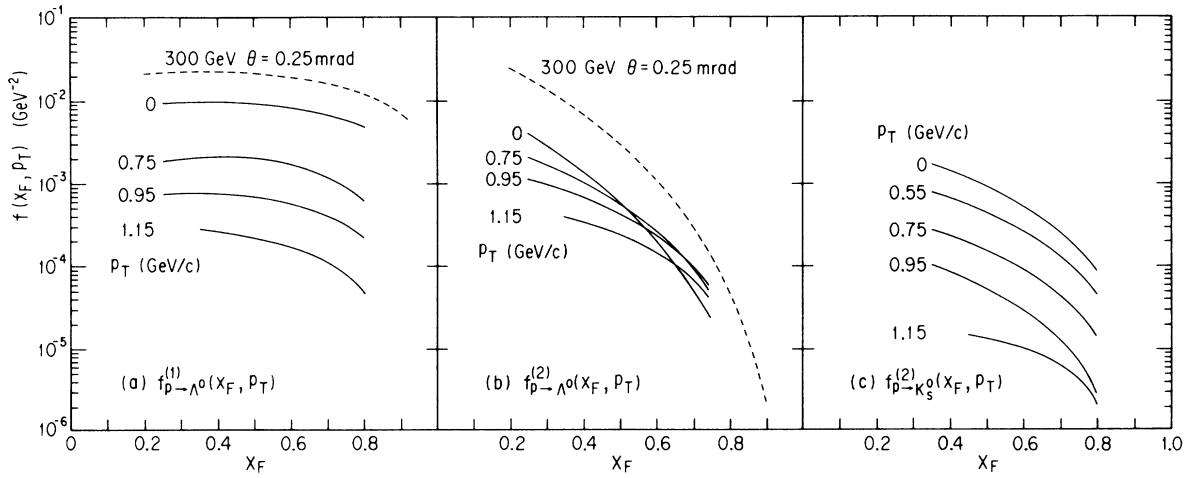

FIG. 18. The (x_F,p_T) distribution functions in the constituent-quark model: (a) $f^{(1)}_{p\to\Lambda^0}(x_F,p_T)$, (b) $f^{(2)}_{p\to\Lambda^0}(x_F,p_T)$, and (c) $f^{(2)}_{p\to K^0_S}(x_F,p_T)$. The uncertainties are large ($\sim 100\%$) for high p_T (see text). The results of Ref. 9 on Λ^0 production by 300-GeV protons are shown by dashed lines.

Analysis by Eq. (9) with the functional form $ax_F{}^b(1-x_F)^c$ assumed for the distribution functions was then found to give satisfactory fits to the measured Λ^0 and Ξ^0 spectra.

The present data at 12 GeV were analyzed by using the cross sections σ_{pA} of Denisov *et al.*[22] and the probabilities $P^{(i)}_{pA}$ of Takagi[9] (see Table VIII). This seems to be a good approximation since the inelastic total cross sections σ_{pA} and $\sigma_{\pi A}$ remain approximately constant above the 10-GeV region. At fixed p_T we parametrized $f^{(1)}_{p\to\Lambda^0}(x_F,p_T)$ in the form $ax_F{}^b(x_0-x_F)^c$ and $f^{(2)}_{p\to\Lambda^0}(x_F,p_T)$ in the form $d(x_0-x_F)^e$. We then fitted the Λ^0 production cross sections on Be, Cu, and W to Eq. (9) and determined the parameters a–e at each p_T. The target-to-target systematic error of 9% was taken into account in the fits. The results of the fits are given in Table IX. The χ^2 values in the fits indicate that Eq. (9) describes the present data reasonably well.

The distributions $f^{(1)}_{p\to\Lambda^0}(x_F,p_T)$ and $f^{(2)}_{p\to\Lambda^0}(x_F,p_T)$ obtained are shown as a function of x_F for several values of p_T between 0 and 1.15 GeV/c in Figs. 18(a) and 18(b). The uncertainty in $f^{(1)}_{p\to\Lambda^0}(x_F,p_T)$ roughly ranges from 20% at $p_T=0$ to 100% at $p_T=1.15$ GeV/c, and that in $f^{(2)}_{p\to\Lambda^0}(x_F,p_T)$ is 40% at smaller x_F and more than 100% at larger x_F. Also shown by the dashed curves are the results of Takagi[9] for the Fermilab data at $\theta=0.25$ mrad,[11] which can safely be regarded as the values at $p_T=0$. The x_F dependences of $f^{(1)}_{p\to\Lambda^0}(x_F,p_T=0)$ and $f^{(2)}_{p\to\Lambda^0}(x_F,p_T=0)$ at 12 GeV are similar in shape to those at 300 GeV. The absolute values of $f^{(1)}_{p\to\Lambda^0}(x_F,p_T=0)$ ($f^{(2)}_{p\to\Lambda^0}(x_F,p_T=0)$) at 12 GeV are smaller than the 300-GeV values by a factor of about 2 (5). This reflects the fact that the 12-GeV region is below the Feynman scaling limit for Λ^0 production.[14,31] The difference of factors 2 and 5 is consistent with the observation[14] that the Feynman scaling is achieved from larger x_F, since $f^{(1)}_{p\to\Lambda^0}(x_F,p_T)$ is more important than $f^{(2)}_{p\to\Lambda^0}(x_F,p_T)$ at large x_F, as can be seen in Figs. 18(a) and 18(b).

Fast K^0_S mesons are produced in the fragmentation or recombination of a single leading quark even if there are two leading quarks. The cross section for K^0_S production is then written[7] by

$$\frac{1}{\sigma_{pA}}E\frac{d^3\sigma}{dp^3}(x_F,p_T;A) = P^{(1)}_{pA}f^{(1)}_{p\to K^0_S}(x_F,p_T)+P^{(2)}_{pA}f^{(2)}_{p\to K^0_S}(x_F,p_T)\ , \quad (11a)$$

TABLE IX. Fits of the (x_F,p_T) distribution functions for Λ^0 production to the Be, Cu, and W data:

$$f^{(1)}_{p\to\Lambda^0}(x_F,p_T)=ax_F{}^b(x_0-x_F)^c,\quad f^{(2)}_{p\to\Lambda^0}(x_F,p_T)=d(x_0-x_F)^e\ .$$

The errors include the systematic uncertainty of 9%. The last column indicates the reduced χ^2 in the fits.

p_T (GeV/c)	a (GeV^{-2})	b	c	d (GeV^{-2})	e	χ^2/DF
0	0.028 3 ±0.003 6	0.59±0.11	1.04±0.11	0.016 ±0.010	4.7 ±1.5	16/34
0.65	0.007 3 ±0.002 4	0.42±0.23	0.84±0.14	0.007 6 ±0.002 9	2.75±0.90	3.9/7
0.75	0.015 1 ±0.009 5	1.13±0.38	1.52±0.39	0.006 3 ±0.002 1	2.92±0.80	3.6/7
0.85	0.006 7 ±0.002 9	0.87±0.31	1.28±0.21	0.004 3 ±0.001 3	2.23±0.50	4.2/7
0.95	0.002 8 ±0.001 1	0.63±0.33	1.08±0.14	0.002 8 ±0.001 0	2.07±0.54	2.4/7
1.05	0.002 0 ±0.001 9	0.58±0.64	1.22±0.48	0.001 30±0.000 48	1.35±0.39	4.0/7
1.15	0.000 56±0.000 42	0.10±0.61	0.85±0.28	0.001 10±0.000 37	1.46±0.30	1.2/4

with

$$f^{(1)}_{p\to K^0_S}(x_F,p_T)=\gamma f^{(2)}_{p\to K^0_S}(x_F,p_T)\ . \tag{11b}$$

The function $f^{(2)}_{p\to K^0_S}(x_F,p_T)$ describes the (x_F,p_T) distribution for K^0_S's that are produced in the fragmentation or recombination of a single leading quark. The constant γ in Eq. (11b) allows for a difference between the probability for a leading single quark to hadronize into a K^0_S and that for a leading diquark. If one assumes that two quarks in the leading diquark hadronize into a K^0_S independently,[5–7] then γ is equal to 2. Determination of γ through least-χ^2 fits of the present data turned out to be difficult, since the optimum γ ranged from 0.6 to 4.0 depending on p_T. In the following analysis we assumed $\gamma=2$ as in Refs. 5–7.

Equations (11) have a characteristic feature that the A dependence and the (x_F,p_T) dependence are factorized. This means that the (x_F,p_T) distribution of K^0_S's produced on nuclei does not depend on A. As mentioned in Sec. IV A, the slope parameters $b(x_F)$ of the p_T dependence differ slightly for Be, Cu, and W targets. Equations (11) thus fail in describing a full detail of the present data on K^0_S production. Neglecting the small discrepancy, we parametrized $f^{(2)}_{p\to K^0_S}(x_F,p_T)$ in the form $a(x_0-x_F)^b$ and determined the parameters a and b by fitting the Be, Cu, and W data to Eqs. (11). An alternative method, for example, determination of $f^{(2)}_{p\to K^0_S}(x_F,p_T)$ from the Be data alone, does not alter the main conclusions of our results. The results of the fits are given in Table X, together with the χ^2 values.

The distribution $f^{(2)}_{p\to K^0_S}(x_F,p_T)$ obtained is shown as a function of x_F for several values of p_T in Fig. 18(c). The uncertainty in $f^{(2)}_{p\to K^0_S}(x_F,p_T)$ roughly ranges from 30% at $p_T=0$ to 80% at $p_T=1.15$ GeV/c. The x_F dependence of $f^{(2)}_{p\to K^0_S}(x_F,p_T)$ shows a steep fall with increasing x_F and is similar to that of $f^{(2)}_{p\to\Lambda^0}(x_F,p_T)$, although the p_T dependence is different.

In a similar manner as in Eq. (9), the p_T-integrated spectra for Λ^0 production can be written by the expression

$$\frac{1}{\sigma_{pA}}\int dp_T{}^2 E\frac{d^3\sigma}{dp^3}(x_F,p_T;A) = P^{(1)}_{pA}g^{(1)}_{p\to\Lambda^0}(x_F)+P^{(2)}_{pA}g^{(2)}_{p\to\Lambda^0}(x_F)\ , \tag{12}$$

where the x_F distribution $g^{(i)}_{p\to\Lambda^0}(x_F)$ is related to $f^{(i)}_{p\to\Lambda^0}(x_F,p_T)$ by

$$g^{(i)}_{p\to\Lambda^0}(x_F)=\int dp_T{}^2 f^{(i)}_{p\to\Lambda^0}(x_F,p_T)\ . \tag{13}$$

The p_T dependence of $f^{(i)}_{p\to\Lambda^0}(x_F,p_T)$ at fixed x_F was well reproduced by the form $a\exp(bp_T+cp_T{}^2)$ (Ref. 20). By means of this parametrization the integral in Eq. (13) was evaluated, yielding the results shown in Fig. 19. The x_F dependence of $g^{(i)}_{p\to\Lambda^0}(x_F)$ was parametrized as

$$g^{(1)}_{p\to\Lambda^0}(x_F)=0.0125x_F{}^{0.68}(1-x_F)^{1.25}\ , \tag{14a}$$

$$g^{(2)}_{p\to\Lambda^0}(x_F)=0.0074(1-x_F)^{2.89}\ . \tag{14b}$$

The powers of $(1-x_F)$ obtained in Eqs. (14) are consistent with the quark-counting rule of Gunion[28] for interactions involving sea quarks which are created from pointlike emitted gluons. At large x_F, the model predicts the x_F distribution $(1-x_F)^1$ for Λ^0's produced in the fragmentation of a leading diquark and $(1-x_F)^3$ for Λ^0's produced in the fragmentation of a leading single quark.

For proton-nucleon collisions, we have $P^{(1)}_{pp}=1$ and $P^{(2)}_{pp}=0$ from the quark-additivity approximation. Thus $g^{(1)}_{p\to\Lambda^0}(x_F)$ is to represent the x_F distribution of Λ^0's in pp collisions. The cross sections for Λ^0 production by 12-GeV protons on hydrogen were measured in the previous experiment[15] by subtraction of Λ^0 yields on polyethylene and carbon targets. The p_T-integrated spectra of Ref. 15 are normalized by the pp inelastic cross section[9]

TABLE X. Fits of the (x_F,p_T) distribution function for K^0_S production to the Be, Cu, and W data:

$$f^{(2)}_{p\to K^0_S}(x_F,p_T)=a(x_0-x_F)^b\ .$$

The errors include the systematic uncertainty of 9%. The last column indicates the reduced χ^2 in the fits.

p_T (GeV/c)	a (GeV^{-2})	b	χ^2/DF
0	0.005 08 ±0.000 77	2.51±0.18	52/22
0.55	0.002 24 ±0.000 23	2.14±0.09	30/7
0.75	0.000 82 ±0.000 10	2.00±0.11	8/7
0.85	0.000 381±0.000 035	1.64±0.07	11/10
0.95	0.000 360±0.000 060	1.98±0.14	14/7
1.05	0.000 112±0.000 019	1.46±0.11	16/7
1.15	0.000 033±0.000 004	0.79±0.06	14/7

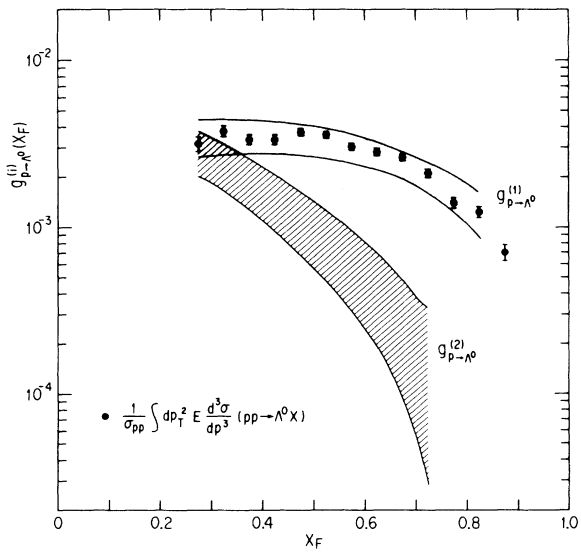

FIG. 19. The x_F distributions $g^{(i)}_{p\to\Lambda^0}(x_F)$ in Λ^0 production. The shaded areas indicate the experimental uncertainties including the systematic errors. The Λ^0 production cross sections on hydrogen (Ref. 15), normalized by the total inelastic cross section $\sigma_{pp}=28.5$ mb, are plotted for comparison.

$\sigma_{pp}=28.5$ mb and are plotted in Fig. 19. Agreement between the experimental data and $g^{(1)}_{p\to\Lambda^0}(x_F)$ is satisfactory. It was observed in Ref. 15 that the $A=1$ cross sections extrapolated by the power law A^α differed from the measured cross sections on hydrogen by a factor of 2. As can be seen from Fig. 19, discrepancies are much smaller in the case of the $A=1$ extrapolation according to the constituent-quark model.

G. Average $p_T{}^2$'s of K^0_S's, Λ^0's, and quarks

The average $p_T{}^2$'s of K^0_S's and Λ^0's were calculated at each x_F by

$$\langle p_T{}^2\rangle=\int p_T{}^2 E\frac{d^3\sigma}{dp^3}dp_T{}^2\Big/\int E\frac{d^3\sigma}{dp^3}dp_T{}^2\simeq\frac{1}{b(x_F)}\ . \tag{15}$$

The integration over $p_T{}^2$ was performed to the kinematic limit, based on the Gaussian p_T dependence Eq. (4) of the cross sections. The results were very nearly equal to $1/b(x_F)$, where $b(x_F)$ was the slope parameter of the p_T dependence. From the x_F dependence of $b(x_F)$ it can be seen that the average $p_T{}^2$'s of K^0_S's and of Λ^0's produced on hydrogen do not depend strongly on x_F, and that the average $p_T{}^2$'s of Λ^0's produced on nuclear targets decrease gradually as x_F increases. As an example, in Fig. 20 we plot the $\langle p_T{}^2\rangle$ of Λ^0's for the W data in comparison with that for the hydrogen data.[15]

In order to interpret the above features in the constituent-quark model, recall that Λ^0 and K^0_S productions in the projectile-fragmentation region are described by the following three processes: (1) hadronization of two leading quarks (a diquark) into Λ^0, (2) hadronization of a leading quark into Λ^0, and (3) hadronization of a leading quark into K^0_S. The (x_F,p_T) dependences of processes (1), (2), and (3) are described by $f^{(1)}_{p\to\Lambda^0}(x_F,p_T)$, $f^{(2)}_{p\to\Lambda^0}(x_F,p_T)$, and $f^{(2)}_{p\to K^0_S}(x_F,p_T)$, respectively. A specific average $p_T{}^2$ can be defined to each of the process (i) by

$$\langle p_T{}^2\rangle_i=\int p_T{}^2 f^{(i)}(x_F,p_T)dp_T{}^2\Big/\int f^{(i)}(x_F,p_T)dp_T{}^2\ , \qquad i=1,2,3\ , \tag{16}$$

where $f^{(i)}(x_F,p_T)$ $(i=1,2,3)$ stand for $f^{(1)}_{p\to\Lambda^0}(x_F,p_T)$, $f^{(2)}_{p\to\Lambda^0}(x_F,p_T)$, and $f^{(2)}_{p\to K^0_S}(x_F,p_T)$, respectively. The $\langle p_T{}^2\rangle$ of Λ^0's is then written by a weighted sum of the average $p_T{}^2$'s in processes (1) and (2), the relative significance of the two processes being dependent on x_F and A:

$$\langle p_T{}^2\rangle_{\Lambda^0}=\frac{P^{(1)}_{pA}g^{(1)}_{p\to\Lambda^0}(x_F)\langle p_T{}^2\rangle_1+P^{(2)}_{pA}g^{(2)}_{p\to\Lambda^0}(x_F)\langle p_T{}^2\rangle_2}{P^{(1)}_{pA}g^{(1)}_{p\to\Lambda^0}(x_F)+P^{(2)}_{pA}g^{(2)}_{p\to\Lambda^0}(x_F)}\ . \tag{17}$$

The $\langle p_T{}^2\rangle$ of K^0_S's is identical to $\langle p_T{}^2\rangle_3$.

The integrals in Eq. (16) were evaluated by means of the parametrization $a\exp(bp_T+cp_T{}^2)$ of $f^{(i)}(x_F,p_T)$ at fixed x_F, similarly as in Eq. (13). The results are shown in Fig. 20. The $\langle p_T{}^2\rangle_1$ does not depend strongly on x_F and is consistent with the measured values[15] of $\langle p_T{}^2\rangle$ of Λ^0's in proton-proton collisions. The $\langle p_T{}^2\rangle_3$ is roughly equal to $\langle p_T{}^2\rangle_1$. The $\langle p_T{}^2\rangle_2$ is significantly larger than $\langle p_T{}^2\rangle_1$ and $\langle p_T{}^2\rangle_3$, although the experimental errors are large, especially at large x_F.

The Ξ^0 hyperons in proton-nucleus collisions are considered to be produced mainly by a process similar to process (2): a leading u quark picks up two s quarks from the sea. We calculated the average $p_T{}^2$ of Ξ^0's in inclusive production by 400-GeV protons on Be using the Fermilab data given in Ref. 12. The results are $0.59-0.65$ $(\mathrm{GeV}/c)^2$ in the range $0.3\le x_F\le 0.7$ and are consistent with our $\langle p_T{}^2\rangle_2$.

From Eq. (17) and the x_F dependences of $g^{(i)}_{p\to\Lambda^0}(x_F)$ illustrated in Fig. 19 we find that, at lower x_F, $g^{(1)}_{p\to\Lambda^0}(x_F)$ and $g^{(2)}_{p\to\Lambda^0}(x_F)$ are in the same order of magnitude and hence processes (1) and (2) contribute roughly equally to the $\langle p_T{}^2\rangle_{\Lambda^0}$ in proton-nucleus collisions, according to the relative weight given by $P^{(1)}_{pA}$ and $P^{(2)}_{pA}$. As x_F increases, however, $g^{(2)}_{p\to\Lambda^0}(x_F)$ falls more rapidly than $g^{(1)}_{p\to\Lambda^0}(x_F)$ and contributions from process (2) become less important, resulting in the gradual decrease of the $\langle p_T{}^2\rangle_{\Lambda^0}$.

In the picture of the constituent-quark model, the transverse momentum of the final-state hadron originates in two separate subprocesses. The leading quark or diquark travels down the nucleus with a certain amount of the transverse momentum, and then hadronizes through fragmentation or recombination to the final-state hadron, acquiring additional transverse momentum kicks. Let the transverse momentum distribution of the leading quarks (diquarks) emerging from the nucleus be Gaussian with a rms spread $\sigma_q(\sigma_d)$. Assume that the transition of a leading quark or diquark to a hadron through picking up a

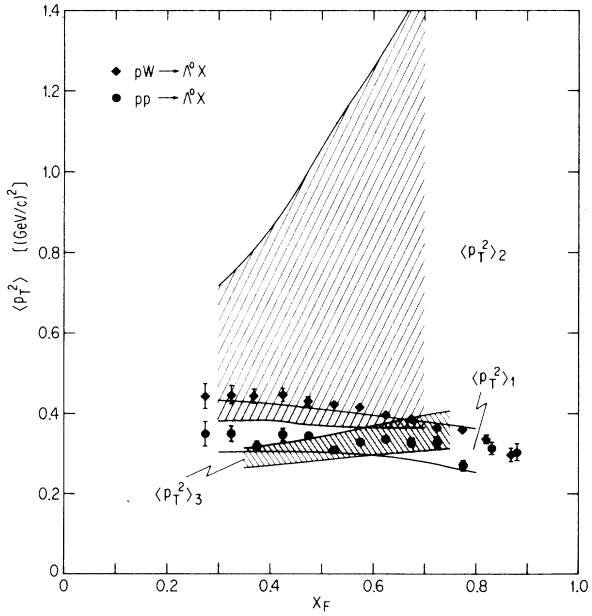

FIG. 20. The average $p_T{}^2$'s in processes (1)–(3): $\langle p_T{}^2\rangle_1$, diquark$\to\Lambda^0$ transition; $\langle p_T{}^2\rangle_2$, quark$\to\Lambda^0$ transition; $\langle p_T{}^2\rangle_3$, quark$\to K^0_S$ transition. The shaded areas indicate the experimental uncertainties including the systematic errors. Also plotted are the average $p_T{}^2$ of Λ^0's on W and that on hydrogen (Ref. 15).

single sea quark (two sea quarks) adds an effective transverse momentum kick, which obeys a Gaussian distribution with a rms spread $\sigma_{1s}(\sigma_{2s})$. Then we have[37]

$$\langle p_T{}^2\rangle_1=(\sigma_d)^2+(\sigma_{1s})^2 , \tag{18a}$$

$$\langle p_T{}^2\rangle_2=(\sigma_q)^2+(\sigma_{2s})^2 , \tag{18b}$$

$$\langle p_T{}^2\rangle_3=(\sigma_q)^2+(\sigma_{1s})^2 . \tag{18c}$$

Substitution of the experimental result $\langle p_T{}^2\rangle_1\simeq\langle p_T{}^2\rangle_3$ in Eqs. (18a) and (18c) yields the relation $\sigma_d\simeq\sigma_q$. The p_T spread of leading diquarks is roughly equal to that of leading single quarks. Using the observation $\langle p_T{}^2\rangle_2 > \langle p_T{}^2\rangle_3$ in Eqs. (18b) and (18c), we find that σ_{2s} is significantly larger than σ_{1s}. The hadronization of leading quarks through picking up two sea quarks results in larger p_T kicks compared with the process of picking up one sea quark.

V. CONCLUSIONS

The cross sections for K_S^0 production by protons incident on nuclear targets (Be, Cu, and W) were measured in the 12-GeV region for the first time. The Λ^0 production cross sections were measured simultaneously. The kinematic range covered was $0.3\le x_F\le 0.8$ and $0.4\le p_T\le 1.3$ GeV/c for K_S^0's and $0.2\le x_F\le 0.9$ and $0.4\le p_T\le 1.7$ GeV/c for Λ^0's. The results were compared with other experiments and were confronted with current theoretical models of hadron production at low transverse momentum. The main conclusions of this experiment are summarized as follows.

(1) The p_T dependences of the K_S^0 and Λ^0 production cross sections are well represented by the Gaussian form $a\exp[-b(x_F)p_T{}^2]$. The slope parameters $b(x_F)$ for K_S^0 production do not depend strongly on x_F, while those for Λ^0 production increase gradually with increasing x_F.

(2) The x_F dependences of the K_S^0 and Λ^0 production cross sections are well represented by the power law $(x_0-x_F)^{m(p_T)}$. The powers m for Λ^0's do not depend strongly on p_T and increase with A. The powers m for K_S^0's appear to decrease with increasing p_T. At small p_T, the powers m are in qualitative agreement with the quark-counting rule of Gunion.[28]

(3) The A dependence of the K_S^0 production cross sections is well represented by the power law $A^{\alpha(x_F,p_T)}$. The exponents $\alpha(x_F,p_T)$ show a trend to increase with p_T. At $p_T=0$, the exponents $\alpha(x_F,p_T=0)$ are consistent with theoretical predictions of the constituent-quark models of Dar and Takagi[5] and of Berlad *et al.*,[6] the dual-parton model of Capella and Tran Thanh Van,[30] and the collective model of Nikolaev and Pokorski.[29]

(4) The cross-section ratios K_S^0/Λ^0 do not depend strongly on A, and decrease at higher x_F and p_T. The x_F dependence of the p_T-integrated cross-section ratios K_S^0/Λ^0 is well represented by a simple exponential function.

(5) Triple-Regge behavior of the $A=1$ extrapolated cross sections for K_S^0 production is consistent with that[35] observed at 300 GeV. The effective Regge trajectory lies between $\Sigma_\alpha-\Sigma_\gamma$ and $\Sigma'_\alpha-\Sigma'_\gamma$ trajectories.

(6) The constituent-quark models[2-9] provide a satisfactory description of the present data. Based on the probabilities $P_{pA}^{(i)}$ given by Takagi,[9] the distribution functions $f^{(1)}_{p\to\Lambda^0}(x_F,p_T)$, $f^{(2)}_{p\to\Lambda^0}(x_F,p_T)$, and $f^{(2)}_{p\to K_S^0}(x_F,p_T)$ are determined. At $p_T=0$, the x_F dependences of $f^{(1)}_{p\to\Lambda^0}(x_F,p_T=0)$ and $f^{(2)}_{p\to\Lambda^0}(x_F,p_T=0)$ are similar in shape to those[9] at 300 GeV. At fixed p_T, $f^{(2)}_{p\to\Lambda^0}(x_F,p_T)$ and $f^{(2)}_{p\to K_S^0}(x_F,p_T)$ fall steeply as x_F increases. The $A=1$ extrapolated cross sections $g^{(1)}_{p\to\Lambda^0}(x_F)$ reproduce the Λ^0 spectra on hydrogen[15] well.

(7) The average $p_T{}^2$'s are evaluated for the diquark$\to\Lambda^0$ transition, the quark$\to\Lambda^0$ transition, and the quark$\to K_S^0$ transition. The quark$\to\Lambda^0$ transition has a significantly larger average $p_T{}^2$ compared with others. These results are used to discuss the average $p_T{}^2$'s of quarks and diquarks involved in the production of K_S^0's and Λ^0's.

ACKNOWLEDGMENTS

We would like to thank T. Nishikawa, S. Suwa, S. Ozaki, and A. Kusumegi for their encouragement throughout the experiment. The experiment would not have been possible without the support of the KEK beam channel group, the KEK accelerator staff, and the KEK radiation safety staff. We wish to thank members of the KEK data handling division and of the machine shop for their kind help. We wish to especially thank L. Pondrom for helpful discussions on hyperon production and F. Takagi for helpful discussions on the A dependence.

*Present address: National Laboratory for High Energy Physics (KEK), Oho-machi, Ibaraki-ken 305, Japan.

†Present address: Institute of Physics, University of Berne, Sidlerstrasse 5, 3012 Berne, Switzerland.

‡Present address: Department of Physics, Chuo University, Kasuga, Bunkyo-ku, Tokyo 112, Japan.

§Present address: Physics Department, Northeastern University, 360 Huntington Ave., Boston, MA 02215.

**Present address: Fermi National Accelerator Laboratory, P.O. Box 500, Batavia, IL 60510.

[1]See, for example, reviews by C. Halliwell, in *Proceedings of the VIII International Symposium on Multiparticle Dynamics,* Kaysersberg, France, 1977, edited by R. Arnold, J.-P. Gerber, and P. Schübelin (Centre de Recherches Nucleaires, Strasbourg, France, 1977), pp. D1–D56; K. Zalewski, in *Proceedings of the X International Symposium on Multiparticle Dynamics,* Goa, India, 1979, edited by S. N. Ganguli, P. K. Malhotra, and A. Subramanian (Tata Institute of Fundamental Research, Bombay, India, 1980), pp. 548–562; A. Białas, in *Multiparticle Dynamics 1982,* proceedings of the XIII International Symposium, Volendam, The Netherlands, edited by W. Kittel, W. Metzger, and A. Stergiou (World Scientific,

Singapore, 1983), pp. 328–358; W. Busza, *ibid.*, pp. 367–373.
[2]V. V. Anisovich, Yu. M. Shabelsky, and V. M. Shekhter, Nucl. Phys. **B133**, 477 (1978).
[3]N. N. Nikolaev and S. Pokorski, Phys. Lett. **80B**, 290 (1979).
[4]A. Białas and E. Białas, Phys. Rev. D **20**, 2854 (1979).
[5]A. Dar and F. Takagi, Phys. Rev. Lett. **44**, 768 (1980).
[6]G. Berlad, A. Dar, and G. Eilam, Phys. Rev. D **22**, 1547 (1980).
[7]F. Takagi, Prog. Theor. Phys. **65**, 1350 (1981).
[8]A. Białas and W. Czyż, Nucl. Phys. **B194**, 21 (1982).
[9]F. Takagi, Phys. Rev. D **27**, 1461 (1983).
[10]K. Heller *et al.*, Phys. Rev. D **16**, 2737 (1977).
[11]P. Skubic *et al.*, Phys. Rev. D **18**, 3115 (1978).
[12]A. Beretvas *et al.*, Phys. Rev. D **34**, 53 (1986).
[13]B. Durand and J. Krebs, Phys. Rev. D **21**, 3137 (1980).
[14]F. Abe *et al.*, Phys. Rev. D **30**, 1861 (1984).
[15]R. Tanaka, Ph.D. thesis, University of Tsukuba, 1984 (unpublished).
[16]F. Abe *et al.*, Phys. Rev. Lett. **50**, 1102 (1983); F. Abe *et al.*, J. Phys. Soc. Jpn. **52**, 4107 (1983).
[17]F. Abe *et al.*, Phys. Rev. D **34**, 1950 (1986).
[18]F. Abe *et al.*, Nucl. Instrum. Methods **220**, 293 (1984).
[19]S. Dhawan, IEEE Trans. Nucl. Sci. **NS-21**, 922 (1974); S. Dhawan, K. Kondo, K. Takikawa, and K. Yasuoka, Jpn. J. Appl. Phys. **23**, 492 (1984).
[20]K. Hara, Ph.D. thesis, University of Tsukuba, 1985 (unpublished).
[21]Particle Data Group, R. L. Kelly *et al.*, Rev. Mod. Phys. **52**, S1 (1980).
[22]S. P. Denisov *et al.*, Nucl. Phys. **B61**, 62 (1973).
[23]P. Bosetti *et al.*, Nucl. Phys. **B54**, 141 (1973).
[24]R. H. Good *et al.*, Phys. Rev. **124**, 1223 (1961); A. Böhm *et al.*, Phys. Lett. **27B**, 594 (1968).
[25]R. T. Edwards *et al.*, Phys. Rev. D **18**, 76 (1978).
[26]G. J. Bobbink *et al.*, Nucl. Phys. **B217**, 11 (1983).
[27]For a review of low-p_T hadron production, see, for example, K. Fiałkowski and W. Kittel, Rep. Prog. Phys. **46**, 1283 (1983).
[28]J. F. Gunion, Phys. Lett. **88B**, 150 (1979).
[29]Nikolaev and Pokorski (Ref. 3); their results are presented in terms of the difference $\alpha(x_F)-\alpha_0$; we used $\alpha_0=0.695$ from Ref. 22.
[30]A. Capella and J. Tran Thanh Van, Z. Phys. C **10**, 249 (1981); the numerical values were calculated by reading their fitted curves for K_S^0 production cross sections on Be and Pb.
[31]V. Blobel *et al.*, Nucl. Phys. **B69**, 454 (1974).
[32]K. Jaeger *et al.*, Phys. Rev. D **11**, 1756 (1975).
[33]A. H. Mueller, Phys. Rev. D **2**, 2963 (1970); C. E. DeTar *et al.*, Phys. Rev. Lett. **26**, 675 (1971).
[34]S. N. Ganguli and D. P. Roy, Phys. Rep. **67C**, 201 (1980).
[35]T. Devlin *et al.*, Nucl. Phys. **B123**, 1 (1977).
[36]K. L. Mir and J. K. Storrow, Z. Phys. C **18**, 47 (1983).
[37]The p_T spread σ_{1s} of sea quarks in Eq. (18a) may be slightly different from that in Eq. (18c) since process (1) includes a transition $uu\to\Lambda^0$ with one of the u quarks being not used in the final Λ^0. This difference, however, should be small because the main contribution to $f^{(1)}_{p\to\Lambda^0}(x_F,p_T)$ is the $ud\to\Lambda^0$ transition above moderate x_F.